# CRYSTAL GROWTH AND RADIATION-INDUCED DEFECTS OF RARE EARTH DOPED LITHIUM YTTRIUM FLUORIDE LASER HOST MATERIALS

By

DAVID WAYNE HART

Bachelor of Science
Southwestern Oklahoma State University
Weatherford, Oklahoma
1984

Master of Science
Oklahoma State University
Stillwater, Oklahoma
1987

Submitted to the Faculty of the
Graduate College of the
Oklahoma State University
in partial fulfillment of
the requirements for
the Degree of
DOCTOR OF PHILOSOPHY
December 1991

CRYSTAL GROWTH AND RADIATION-INDUCED

DEFECTS OF RARE EARTH DOPED

LITHIUM YTTRIUM FLUORIDE

LASER HOST MATERIALS

Thesis Approved:

Joel J. Martin

Thesis Adviser

George S. White

Elizabeth M. Holt

Timothy M. Wilson

Richard C. Powell

Thomas C. Collins

Dean of the Graduate College

ACKNOWLEDGMENTS

I extend my sincere appreciation to Professor Joel J. Martin for his help and encouragement throughout my graduate tenure. Without his assistance and his vast knowledge of experimental physics I would not be where I am today. I have enjoyed working for and with him these past years.

My gratitude is expressed to the faculty and staff of the Department of Physics of Oklahoma State University and especially to those members of my committee: Professors George S. Dixon, Elizabeth M. Holt, Richard C. Powell, and Timothy M. Wilson.

I also express my appreciation to Mr. Charles A. Hunt for his technical assistance and the many discussions on the various aspects of crystal growth, Dr. Mahendra Jani for his valuable assistance, and to Mr. Heinz Hall and Mr. Mike Lucas for their expertise in the fabrication of the apparati used in this study.

Finally to the ones most responsible for my accomplishments, my parents Samuel C. and Delores S. Hart for their encouragement and patience throughout these years, and my wife, Debra, with whom I would do it all over again.

This study was sponsored by the Department of Physics

of Oklahoma State University and NASA-Langley from whom I received a Fellowship which aided in continuing my education and personal goals.

TABLE OF CONTENTS

LIST OF TABLES

LIST OF FIGURES

Figure Page

# CHAPTER I

# CRYSTAL GROWTH OF LITHIUM YTTRIUM FLUORIDE

## Introduction

Rare-earth doped lithium yttrium fluoride (YLF) is of interest for use as a mid-infrared solid state laser. The applications of this material range from remote atmospheric sensing to wind shear detection and communications. This material had been and is currently the subject of these research applications. The study of this subject is two-fold, first is the crystal growth of lithium yttrium fluoride using the Czochralski and Bridgman techniques and second is the identification of radiation induced defects in YLF.

Lithium yttrium fluoride crystals, both doped and undoped, have been grown using the Czochralski or crystal pulling and Bridgman or directional freezing techniques.[1,2,3] Crystal growth of lithium yttrium fluoride presented in this study is achieved by both methods and is a semi-detailed record by which single crystals of undoped and rare-earth doped YLF may be grown.

The Bridgman method has shown to be a useful method for obtaining research sized crystals. These crystals are

grown at a rate of 1.5 millimeters per hour and the system used in this study produces crystals with near 100% yield.

The Czochralski method is a somewhat difficult technique for growing YLF in that the crystal must be grown in excess LiF. This method has been shown to produce large, oriented crystals, in comparison with the Bridgman grown crystals. However, due to the difficulty in growing crystals by this technique and the need to rapidly provide small research samples with different dopants Bridgman growth is the preferred method.

## The Phase Diagram of YLF and Crystal Growth Using Melt Techniques

The phase diagram of the system $LiF-YF_3$, shown in Figure 1, was determined by Thoma, et. al.[4] from thermal analysis of heating and cooling curves and from the identification of phases in quenched samples. The system has two invarient points at 19% (mole percentage) $YF_3$ and 695°C and at 49% $YF_3$ and 819°C. At compositions less than 19% $YF_3$ (mole percentage) the primary phase, that phase which first appears on cooling the molten material, is crystalline LiF. While at compositions greater than 48% $YF_3$, the primary phases are the polymorphic forms of $YF_3$. The single intermediate compound $LiF \cdot YF_3$ (lithium yttrium fluoride: $LiYF_4$, YLF) is the primary phase at compositions between these two points of invariance.

Lithium yttrium fluoride (YLF) melts incongruently at

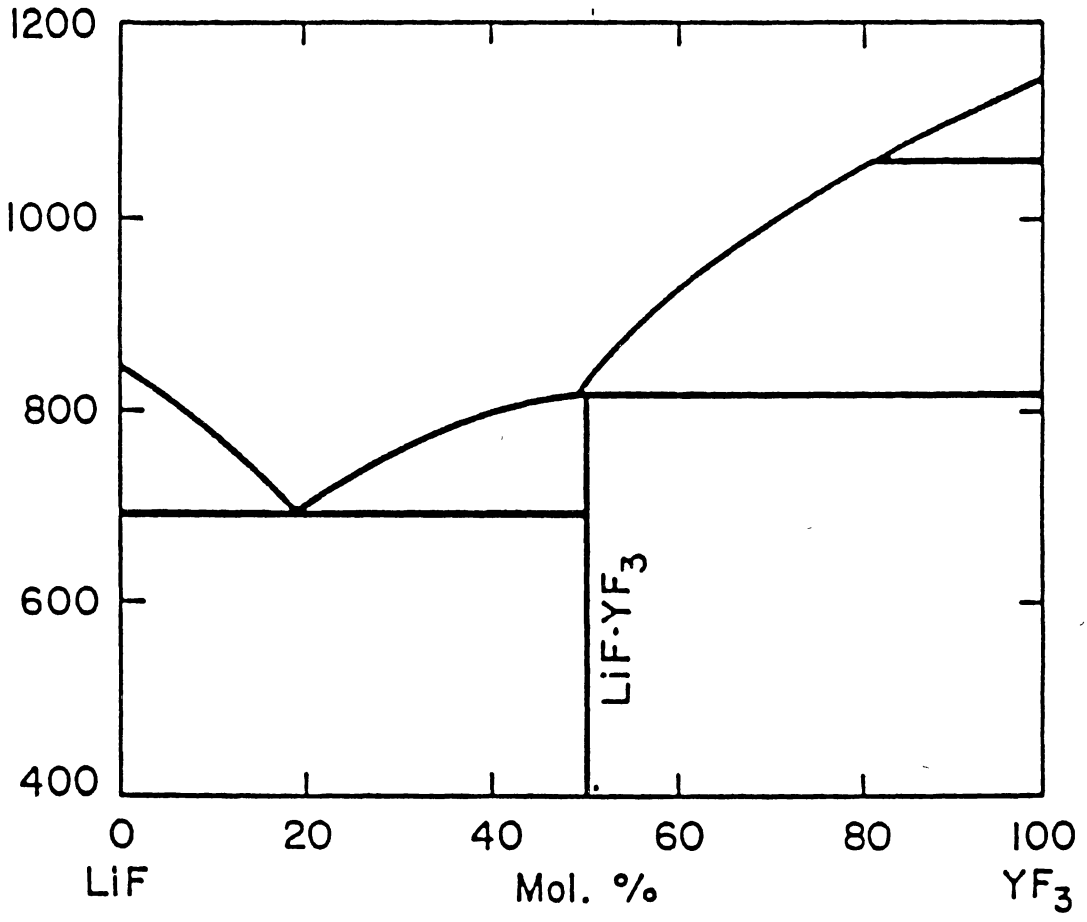


Figure 1. Phase Diagram of the System LiF-$YF_3$

819°C to $YF_3$ and liquid. Consequently, crystal growth of this compound must be performed from a solution containing excess LiF to avoid precipitation of $YF_3$. The most convenient composition is 48% $YF_3$ and 52% LiF.

The two techniques by which YLF has been grown are the Czochralski, or crystal pulling, and the Bridgman, or directional freezing, techniques. The Bridgman technique works by passing a crucible containing the growth material through a temperature gradient at the melting point. This technique has an advantage over the Czochralski technique in that it is more of a hands-off method crystal growth. Once the growth parameters (temperature, pressure, and growth rate) are determined, manual operation of a particular system is limited to starting and stopping the growth procedure.

The Czochralski technique is probably the most widely used melt growth technique since single crystals of known orientation can be obtained. The method involves placing the growth material into an open mouthed crucible, melting the material, then seeding the molten material with a seed inserted into the exposed free surface. A crystal is then pulled from the melt by raising the seed. The difficulty arises in the insertion of the seed into the melt, then keeping the temperature at the seed/crystal-melt interface at the nucleation point of the material. Hence the main problem is one of thermal gradients.

The various techniques used to smooth temperature

gradients are usually determined by trial and error. However, techniques used in previous crystal growth experiments provide a basis for determining a methodology of growing a particular crystal.

# CHAPTER II

# EXPERIMENTAL PROCEDURE

## Hydrofluorination of the Growth Material

In previous attempts to grow YLF by the Czochralski and Bridgman techniques the resulting boule was colorless but was invariably polycrystalline and opaque. At the time it was uncertain whether the boule was polycrystalline because of the "opaqueness" or was polycrystalline due to the growth parameters (temperature, pressure, growth rate) employed at the time with the lack clarity due to contamination of the growth material. The material used to grow the boules consisted of high purity (99.99%) yttrium and rare-earth fluorides and optical grade LiF crystals. However due to the lack of clarity in the boules, a hydrofluorination system was setup to treat the growth material in an effort to remove any oxides, hydroxide, or oxyfluorides which may have formed during processing and storage of the growth material. Undoped crystals of YLF grown after HF treatment of the growth material were invariably clear and colorless.

Hydrofluorination has been used for quite some time to purify fluoride compounds and in the conversion of oxide material to fluoride material. The system shown in Figure

2 is designed similar to what was reported earlier by Uhrin and Belt[3] in their study on the preparation and growth of YLF. This hydrofluorination system has undergone somewhat extensive modification since it was first employed. The diagram shown in Figure 2 is the latest version of the system and perhaps the better of all the previous systems. The basic difference between this and the previous systems lies in the method by which the HF gas is introduced into the system. The whole system itself is placed inside a fume hood which provides a measure of isolation from the highly corrosive HF acid.

The reaction tube is made of Inconel which is sealed on both ends with stainless steel flanges and teflon o-rings. This tube is connected to the rest of the system via polypropylene tubing which has good resistance to HF. However, the tubing colors after extended use, necessitating periodical replacement. This polypropylene tubing is connected to the various components of the system using Monel connectors.

The gas mixing chamber is constructed of stainless steel. As mentioned earlier this is the latest modification to the system in general. The gas mixing chamber provides a safety feature in that the HF bottle is open only for a short period of time; long enough to condense a small amount of HF in the mixing chamber.

To treat a given amount of growth material, the material was placed inside a platinum or graphite crucible

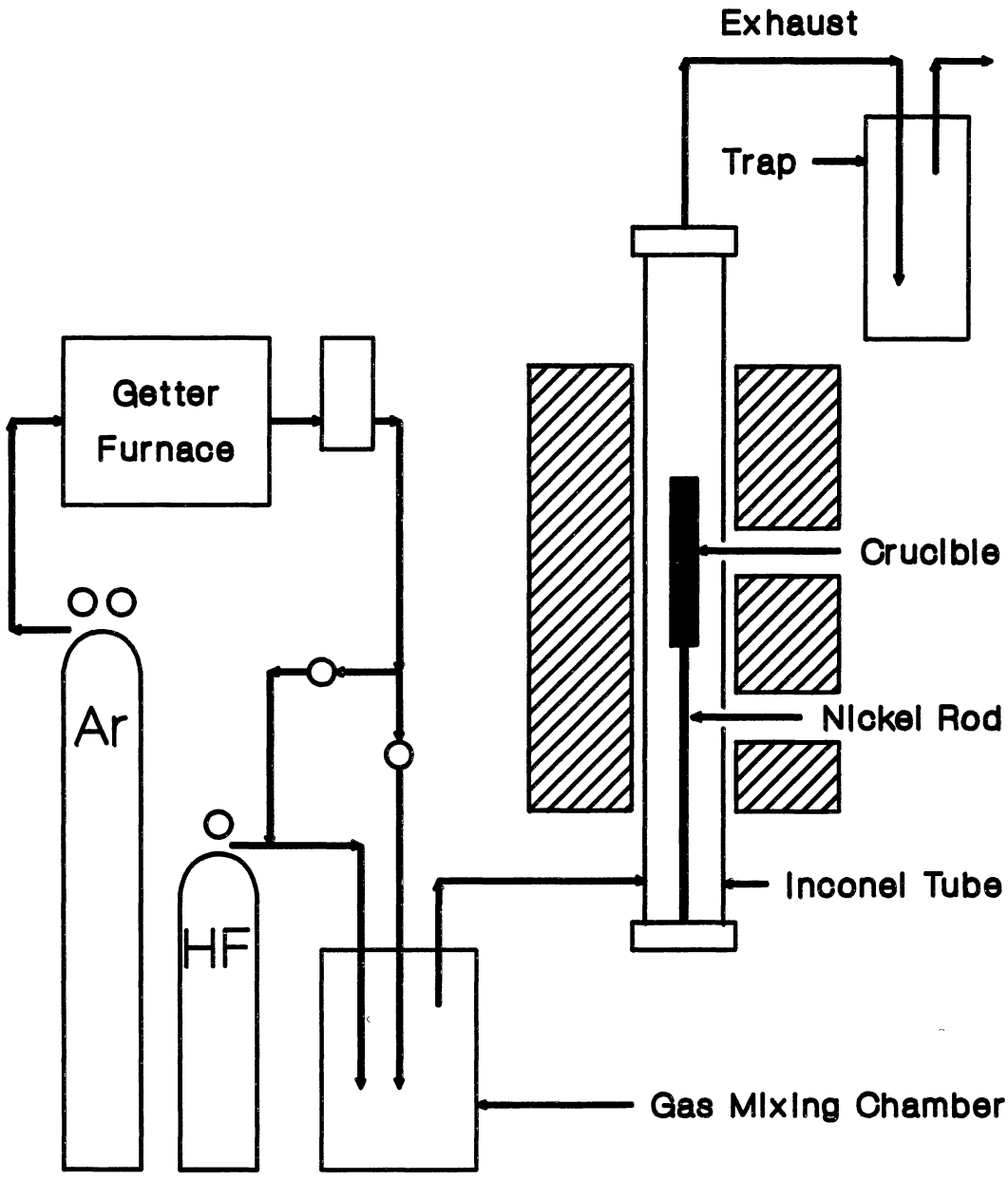


Figure 2. The Hydrofluorination System

with a loose fitting platinum foil cap providing a top cover. A sheath of graphite paper was then inserted into the Inconel reaction tube followed by the crucible itself. After earlier attempts at treating the growth material, the treated material was found to have a greenish hue. Inspection of the reaction tube revealed a greenish material adhering to the inside surface. This material was thought to be nickel fluoride and the graphite sheath and platinum cap are used to isolate the growth material from the contaminant.

Upon insertion of the crucible into the reaction tube, the tube was sealed and placed inside the furnace. After connecting the tube to the rest of the system, gettered argon was used to purge the system. Throughout the hydrofluorination process the argon gas was allowed to flow throughout the whole system.

After purging the system the furnace temperature was elevated to 950°C and HF was introduced into the system. The HF/argon gas passed through the reaction tube then into the first of two sodium bicarbonate/water neutralizing traps which were connected in series. Phenol Red was used as an approximate Ph indicator in the traps.

The length of time the temperature was held at 950°C, with HF passing through the system, varied from 45 minutes to an hour. The temperature was then decreased over a nine hour period during which HF was passed through the system until melting point of YLF was reached.

## Czochralski Growth of Lithium Yttrium Fluoride

A diagram of the Czochralski growth system is shown in Figure 3. Shown are the internal parts of the system which are completely enclosed in water-cooled stainless steel jackets. This growth system operates using a wire mesh tungsten resistance heater. This heater was manufactured in cylindrical halves which are separated by about 1 centimeter and joined at the top. Concentric stainless steel heat reflectors surround the heater and a stainless steel heat reflector covers a majority of the area above the heater.

The vitreous carbon crucible rests on a stainless steel pedestal which rotates at a constant 3 revolutions per minute. That the crucible rotates is important due to the design of the heater. Cool regions near the gaps separating the heater cause undesirable precipitation in the melt if the crucible is not rotated.

The pull rod is constructed of two concentric stainless steel tubes. The outer tube is nickel plated and sealed with a nickel chuck on one end which holds the seed. The inner tube transports water to the seed end of the outer tube as a means to modify the temperature gradient along the seed.

The temperature of the furnace is measured with a Type S (Pt-Pt 10% Rh) thermocouple (TC) that is pressed against the heater and positioned horizontally with the midpoint of the crucible. The heater may be controlled by two

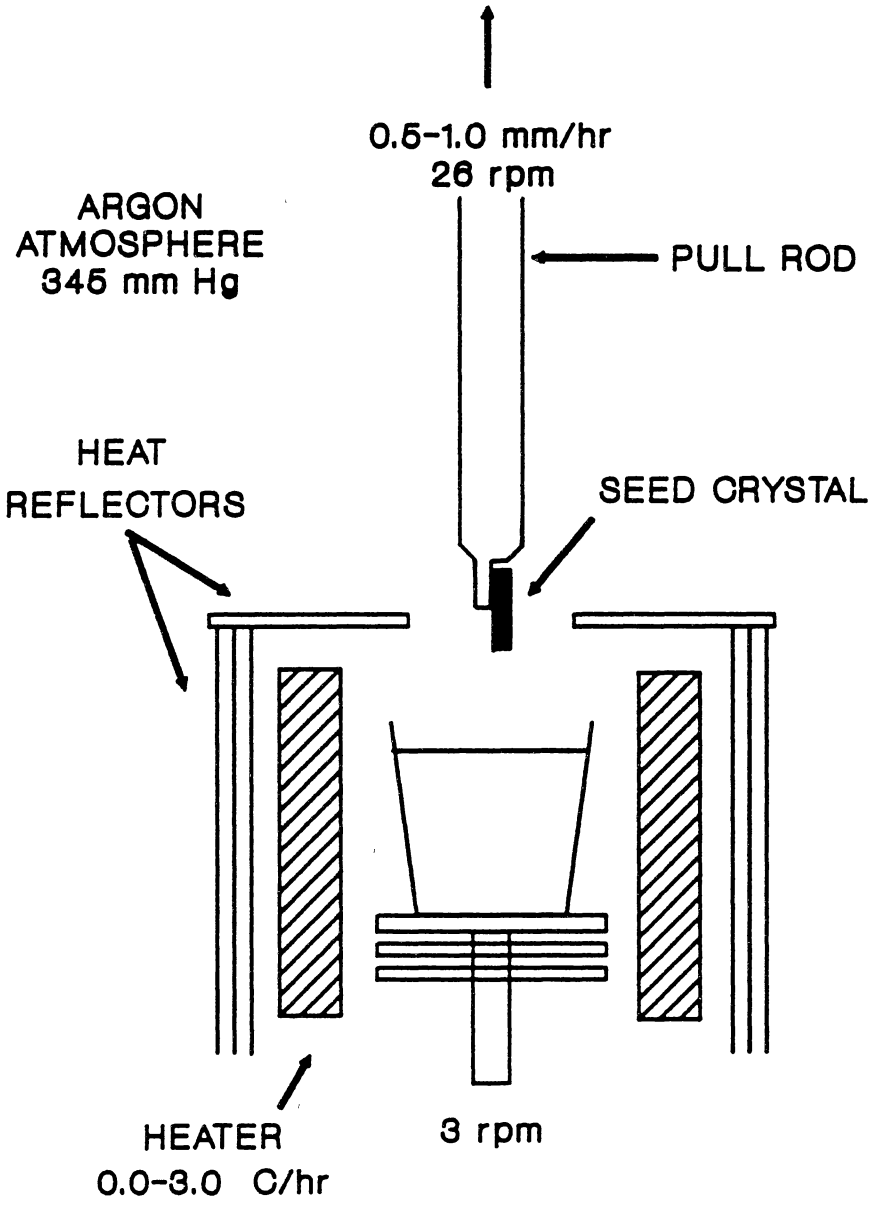


Figure 3. The Czochralski Growth System

different furnace controllers, Figure 4, which may be operated manually via front panel controls or remotely. The output of the primary furnace controller is gauged by the emf of the thermocouple in either the remote or manual modes. In the remote mode of the primary controller, the secondary controller determines the setpoint (temperature).

The secondary controller is interfaced to a computer via a relay box. The computer monitors the temperature of the system by reading the emf of the TC directly from the digital multimeter (DMM) and can increase or decrease the temperature of the heater by actuating the appropriate switches in the relay box. The computer also accumulates temperature and time data of the crystal growth process.

The power supply, which is interfaced with the computer, has a resolution of 2 microvolts and is placed in series with the thermocouple. Hence the power supply/computer combination provides a method of increasing or decreasing the temperature of the system smoothly over a period of time. By adding a small voltage to the emf of the thermocouple the controller reads a change in temperature and decreases or increases the output to the heater. For growth of YLF crystals, the incremental changes in temperature range from 0.5 to 3 degrees per hour.

With the crucible in place and the system sealed, the growth chamber was evacuated using a high vacuum pumping system. A leak check was performed at this point by

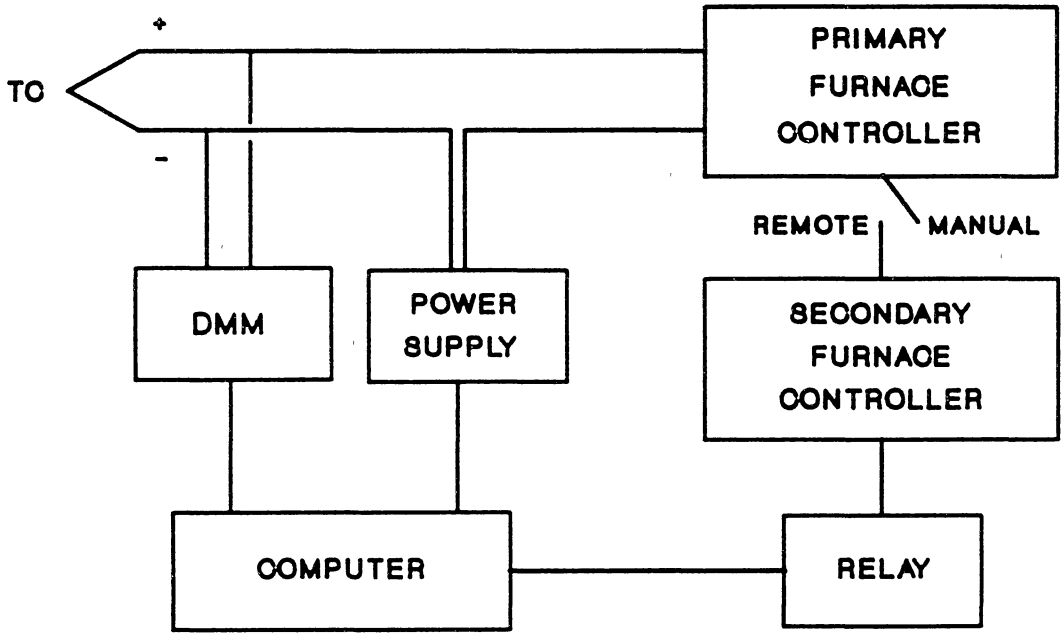


Figure 4. Schematic of the Temperature Control System of the Czochralski Growth System

isolating the system from the pumping after a sufficiently low pressure was attained. If no leaks were apparent, the system was opened to the vacuum pumping system and the temperature was elevated, using the secondary furnace controller, to a temperature of 450°C. After a period of at least four hours the system was backfilled to a pressure of 310 mm Hg with gettered argon.

At this point a second leak check was performed. If no leaks were apparent, the temperature was then increased to 860°C. The pressure at 860°C was 345 mm Hg. At this point the furnace controller was switched to the primary controller; the primary controller gave better manual control over the heater than the secondary controller.

In most cases the top of the melt was covered with slag. Most of the slag is thought to be graphite from the sheath used during hydrofluorination of the growth material and from the vitreous carbon crucible. If the slag coated the whole surface area of the melt, the furnace was cooled to room temperature and the slag was removed. In past growth attempts a large quantity of slag caused polycrystalline growth; in all growth attempts there was always some slag on the surface.

The seed was rotated at a rate of 26 rpm during the whole growth procedure and was dipped into the melt at about 832°C. Shown in Figure 5 is the temperature and time data for the whole growth procedure. The large temperature changes are due to the changes in the setpoint using the

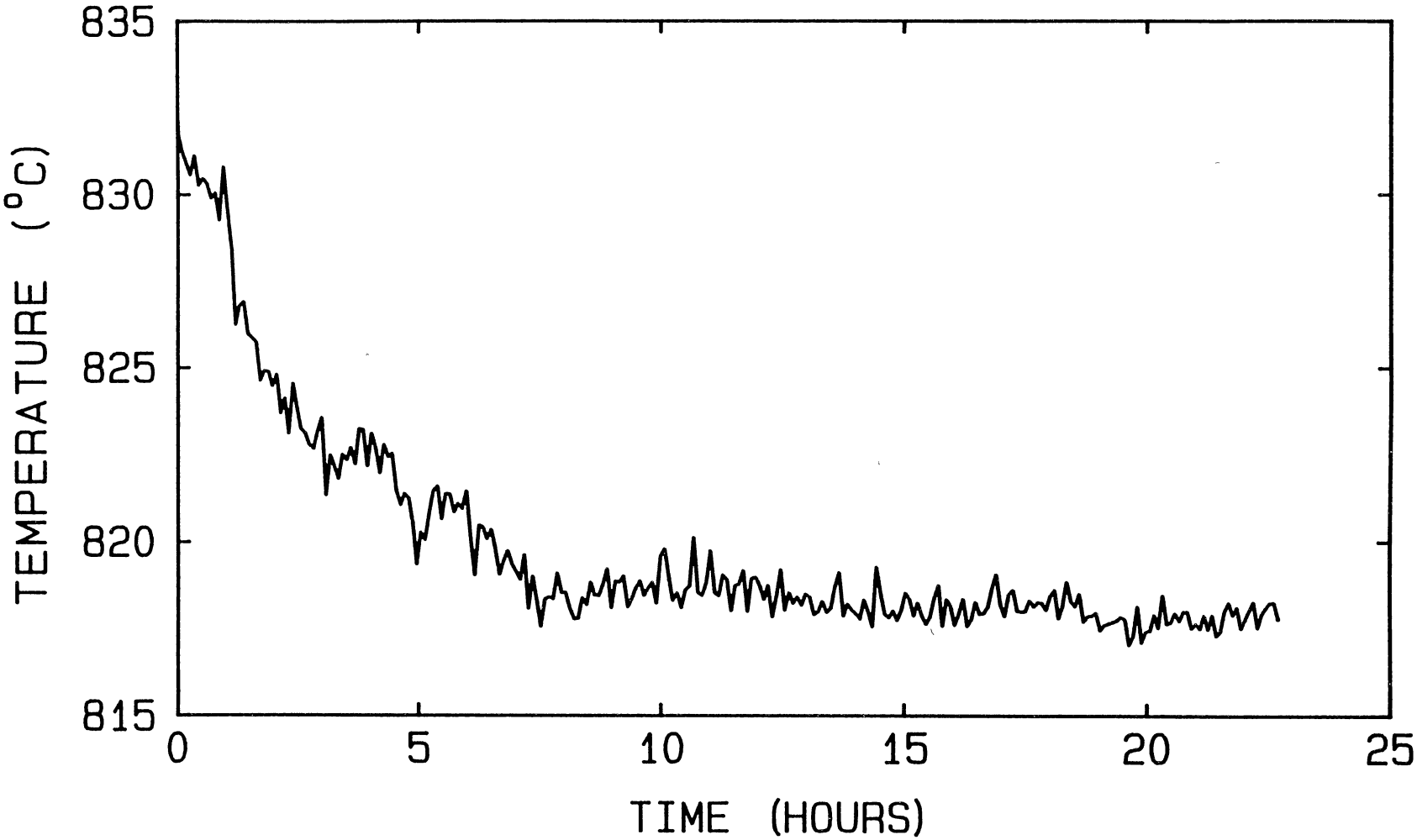


Figure 5. Temperature Profile for Crystal Growth of Lithium Yttrium Fluoride Using the Czochralski Growth System

manual controls of the primary controller. The slow decreases in temperature were controlled by the computer.

Throughout the whole growth process the rate at which the crystal was pulled from the melt was varied from 0.5 mm/hr at the start of the growth process to 1 mm/hr as the diameter of the crystal increased. However due to the tapered geometry of the crucible, the growth rate is approximately 1.5 mm/hr. During a majority of the growth procedure the temperature was roughly 818°C.

## Bridgman Growth of Lithium Yttrium Fluoride

A diagram of the Bridgman system which utilizes the vertical Bridgman technique is shown in Figure 6. With the appropriate growth parameters this system produces YLF crystals with near 100% yield. The system consists of a furnace and programmable temperature controller. The crystal is grown in a vitreous carbon crucible that is supported in the system by a graphite and nickel pedestal. An alumina tube is used to isolate the crucible from the outside environment. A motorized platform supports the growth chamber and is capable of moving at rates ranging from 0.03 to 1.5 millimeters per hour.

The lower part of the growth chamber supports a pressure gauge, a valved vacuum feedthrough and a thermocouple feedthrough for a Type S (Pt-Pt 10%Rh) thermocouple.

As indicated by the drawing, the crucible is divided

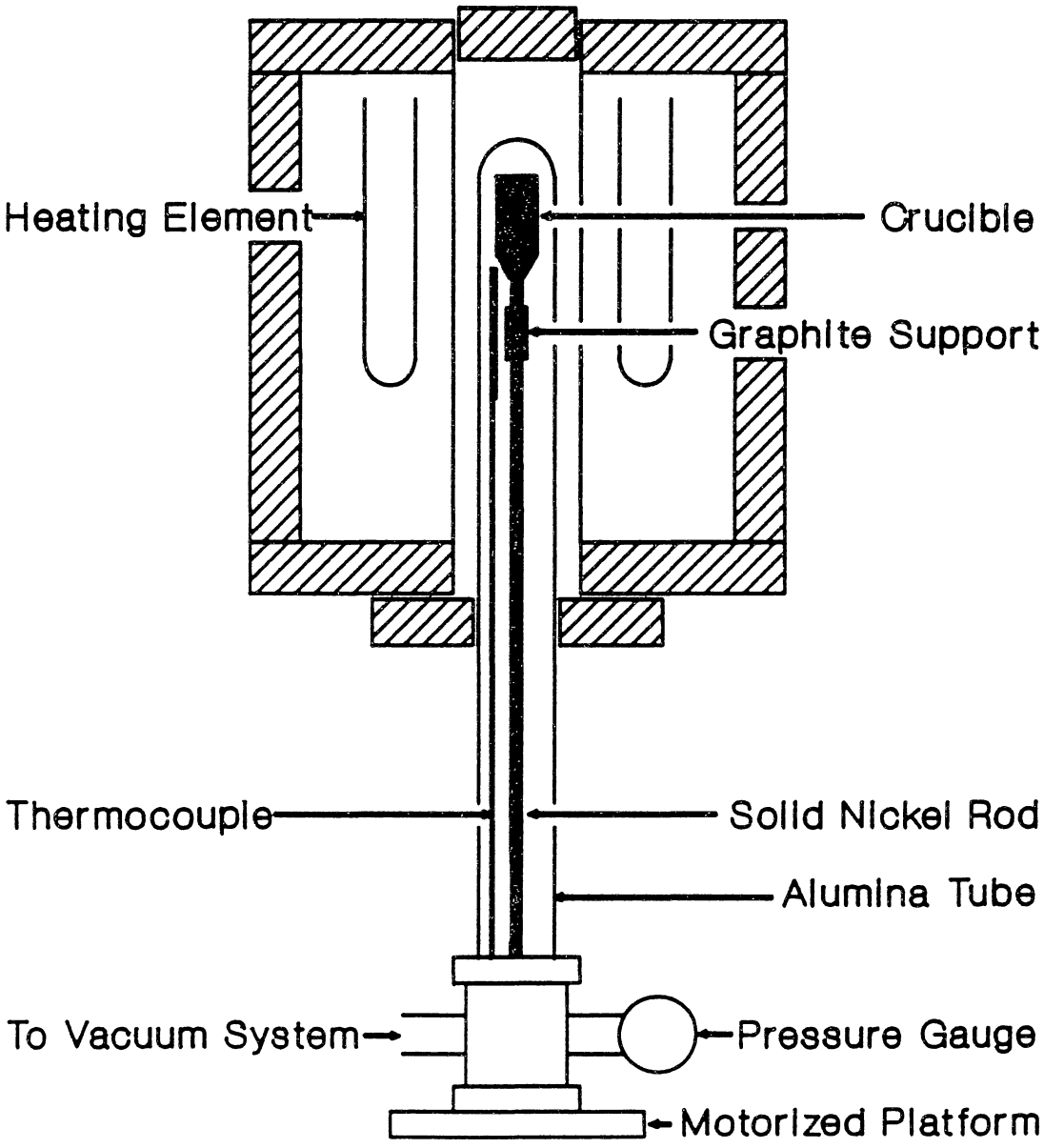


Figure 6. The Bridgman Growth System

into three regions. The bottom region is the seed region. It is cylindrical with an inside diameter of 2.5 millimeters and is 7.5 millimeter is length. The middle region is conical with an angle of about 30° and the top region in cylindrical with an inside diameter of 13.5 millimeters.

In most cases the growth material was taken directly from the hydrofluorination system to the growth system in an effort to limit the amount of absorbed and/or adsorbed contaminants. Before placing the growth material into the vitreous carbon crucible, the material was broken into pieces just large enough to fit into the crucible; only a small amount of the material was powdered.

Despite the efforts, it was highly probable that the material absorbed contaminants during the transition of the growth material from the hydrofluorination system to the growth system. Consequently, $NH_4HF_2$ was added to the growth material after the material was placed in the crucible. Ammonium hydrogen fluoride is the agent of choice in converting $Y_2O_3$ to $YF_3$.[4] Though it is unlikely that $Y_2O_3$ was present in the growth material after the HF treatment of the fluoride growth material, $NH_4HF_2$ was added as a precaution.

Upon placing the crucible in the system, a Type S (Pt-Pt 10% Rh) thermocouple was positioned next to the seed region of the crucible. The alumina tube was then placed over the crucible and sealed with a water-cooled double o-

ring vacuum seal. A high vacuum pumping system then evacuated the growth chamber to a pressure on the order of $10^{-6}$ Torr.

Upon attaining a sufficiently low pressure, the furnace temperature was elevated to 450°C with the system under vacuum, and held for a length of time no shorter than 8 hours (overnight). The temperature of 450°C was chosen since the conversion of yttrium oxide to yttrium fluoride occurs in the temperature range of 400-600°C.[4]

Before raising the furnace temperature above 450°C, the growth chamber was isolated from the vacuum system and backfilled to a high pressure (+6 psi or 1070 mm Hg) with anhydrous (gettered) argon. The gas acts as a heat exchange medium and the high pressure insures against losses due to the increase in vapor pressure of the components at elevated temperatures. At the growth temperature of YLF (819°C) the vapor pressure of LiF is less than 1 mm Hg while the vapor pressure of $YF_3$ is less than $10^{-4}$ mm Hg. Shand[2] reported achieving success in Bridgman growth of YLF with a pressure of 500 mm Hg. Consequently a high positive pressure is not necessary, however success with this growth system using this high pressure almost forbids making any adjustment.

Upon backfilling the system, the furnace temperature was then increased to 970°C and held at this temperature throughout the growth process. The temperature profile of the furnace at this temperature is shown in Figure 7 where,

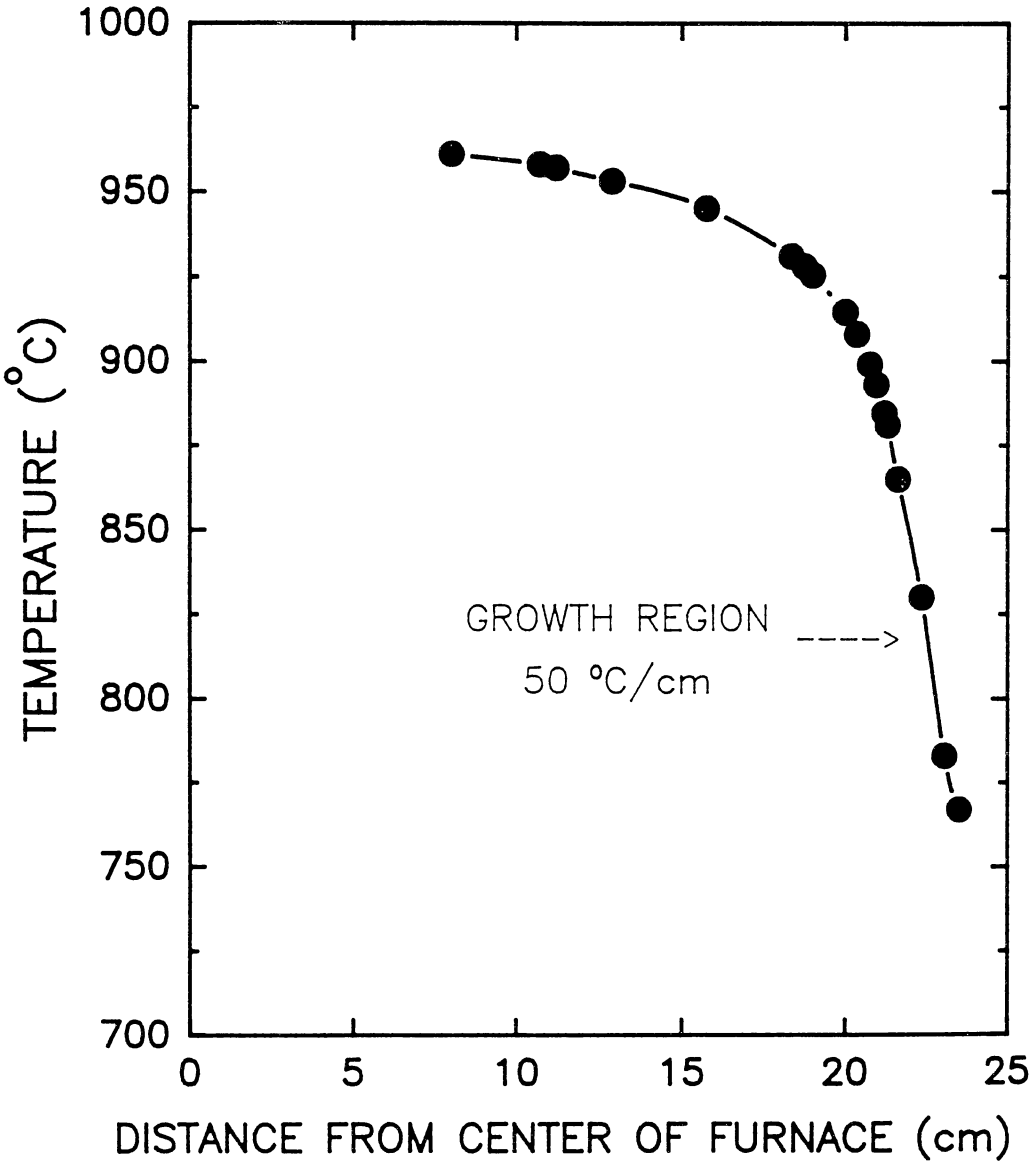


Figure 7. Temperature Profile for Crystal Growth of Lithium Yttrium Fluoride Using the Bridgman Growth System

for lack of a better reference point, the temperature is plotted versus the distance from the center of the furnace. The growth process was started with the bottom of the crucible located about 7 centimeters from the center of the furnace. At this position the temperature is a constant 970°C along the length of the crucible, assuring, at least initially, homogeneity of the melt.

Growth of the crystal was then accomplished by lowering the crucible through the temperature gradient at a rate of 1.5 millimeters per hour. At the nucleation point of YLF (819°C) the temperature gradient is 50°C/cm.

Crystal growth was considered complete when the top of the crucible was below the melting point. However to insure complete solidification, the crucible was lowered until the temperature measured at the seed was below 600°C. The furnace was then cooled to room temperature over a period of 24 hours.

# CHAPTER III

# RESULTS

## Czochralski Grown Lithium Yttrium Fluoride

The Czochralski YLF crystals were grown using an a-axis or [100] seed. The undoped YLF crystals were clear and colorless, 3.5 centimeters in length and had a slight elliptical cross section. All the crystals were concave at the growth interface.

Uhrin and Belt[3] also reported a slight elliptical cross section for crystals grown along [100] and also reported that the c-axis lie along the major axis. This result was confirmed for the crystals grown in this study. Uhrin and Belt also observed a growth ridge along [001] which ran the length of Czochralski grown crystals. This ridge was not seen in the crystals grown in this study, but four ridges were apparent on the top of the boule. These ridges presumably marked the [101] directions.

Concave growth interfaces are usually the result of a fast crystal rotation rate.[5] Consequently the rotation rate may be reduced for growth of YLF. But inspection of a cross sectional slice of the grown crystal did not reveal a high dislocation density which can be a consequence of a fast rotation rate.

In summary, the seed was rotated at a rate of 26 revolutions per minute and the crucible was counter-rotated, with respect to the seed rotation, at a rate of 3 revolutions per minute. The internal pressure during the growth process was 345 mm Hg at a temperature of 818°C. The rate at which the crystal was pulled from the melt varied from 0.5 mm/hr at the start of the process to 1.0 mm/hr as the crystal grew in diameter. The temperature was lowered at rates ranging from 0 to 3 °C/hr. The temperature was held relatively constant during a majority of the growth process as indicated by Figure 5.

Perhaps the only problem limiting the Czochralski growth of YLF was the slag present on top of the melt. As mentioned previously, a majority of the slag was thought to be graphite (carbon). In many cases when a large quantity of slag was present, a fast polycrystalline growth was observed when the seed was placed into the melt.

## Bridgman Grown Lithium Yttrium Fluoride

Each crystal grown by the Bridgman method had a small quantity of slag on the top of the boule and bubbles in the tapered or conical region of the boule. It is not expected that the slag had any effect on the quality of the grown crystal since the Bridgman crystals are grown from the bottom of the melt. It did not appear that the bubbles had any effect on the quality of the grown crystal. Visual observation of the crystal through a conoscope did not

detect any large angle dislocations in the upper cylindrical portion of the boule.

In each single crystal, the c-axis lay at an angle of roughly 30° to the axis of the boule. This angle roughly corresponds to the angle between [001] and [111] which is 33°. Woodruff[6] states that the nucleation rate is proportional to the number of atoms or molecules on a given surface. Hence those surfaces with the largest number of sites on the surface will grow faster. The implication is that the growth will proceed in successive planes of atoms. From a model of YLF, (221) appears to be a candidate for the growth plane. The normal to (221) makes an angle of about 27° to [001]. Hence the normal to (221) is probably the growth direction.

Bridgman crystals were grown singly and doubly doped with dysprosium, holmium, erbium, and thulium. The optical absorbance of samples cut from the top and bottom of a holmium doped crystal indicated uniform doping throughout the crystal. In Figure 8 the melt concentration of holmium is plotted versus the 637 nanometer holmium absorption. These data obey the relation $X_{Ho}=0.276(\alpha_{637})$. In Figure 9 the melt concentration of thulium is plotted versus the 780 nanometer thulium absorption. These data obey the regression relation $X_{Tm}=1.11(\alpha_{780})-0.16$. Hence knowledge of the thulium or holmium absorption coefficients at the appropriate wavelengths in doped YLF crystals give an indication of their respective concentrations.

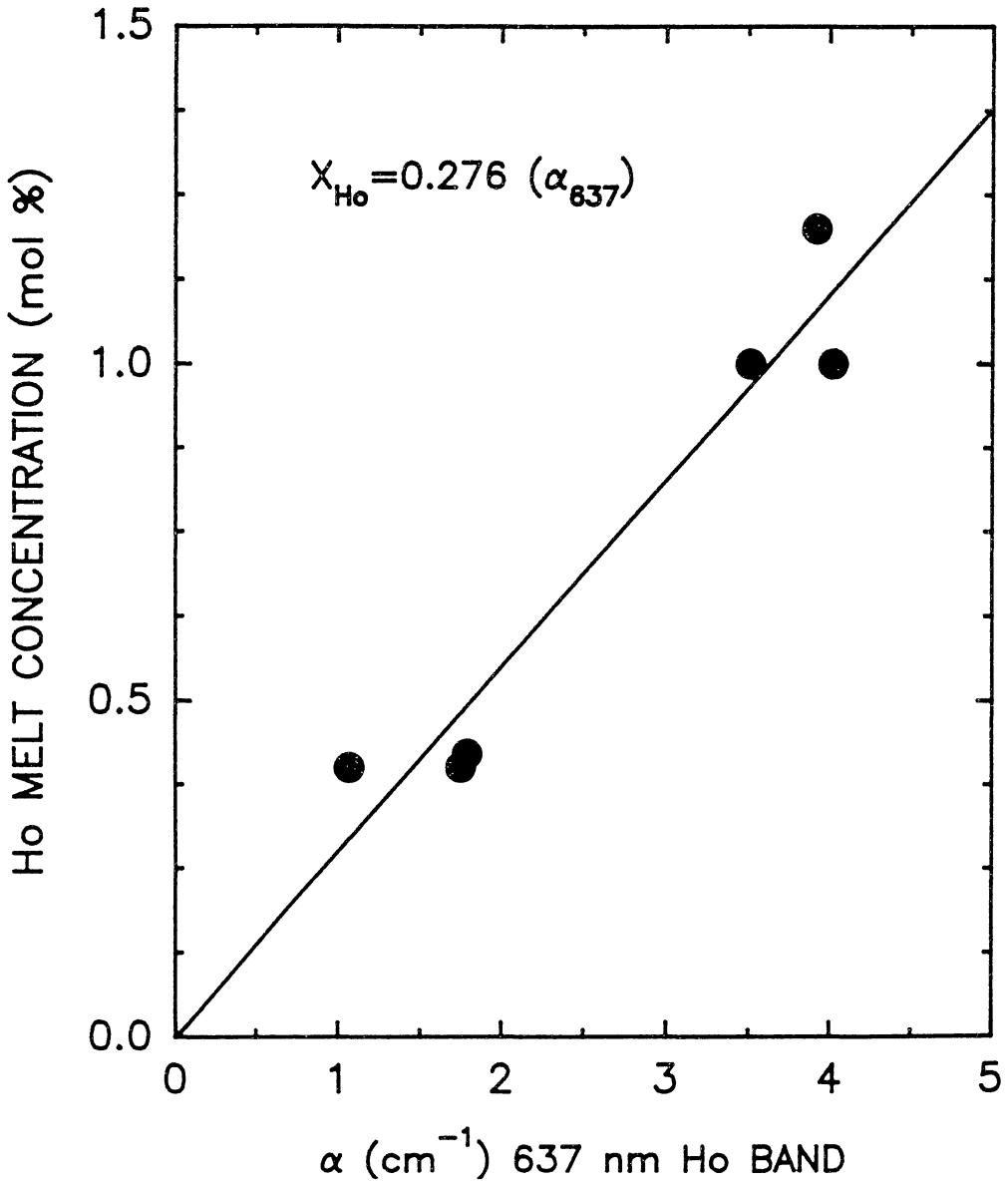


Figure 8. Holmium Concentration as a Function of the Absorption Coefficient of the 780 nm Holmium Absorption Band

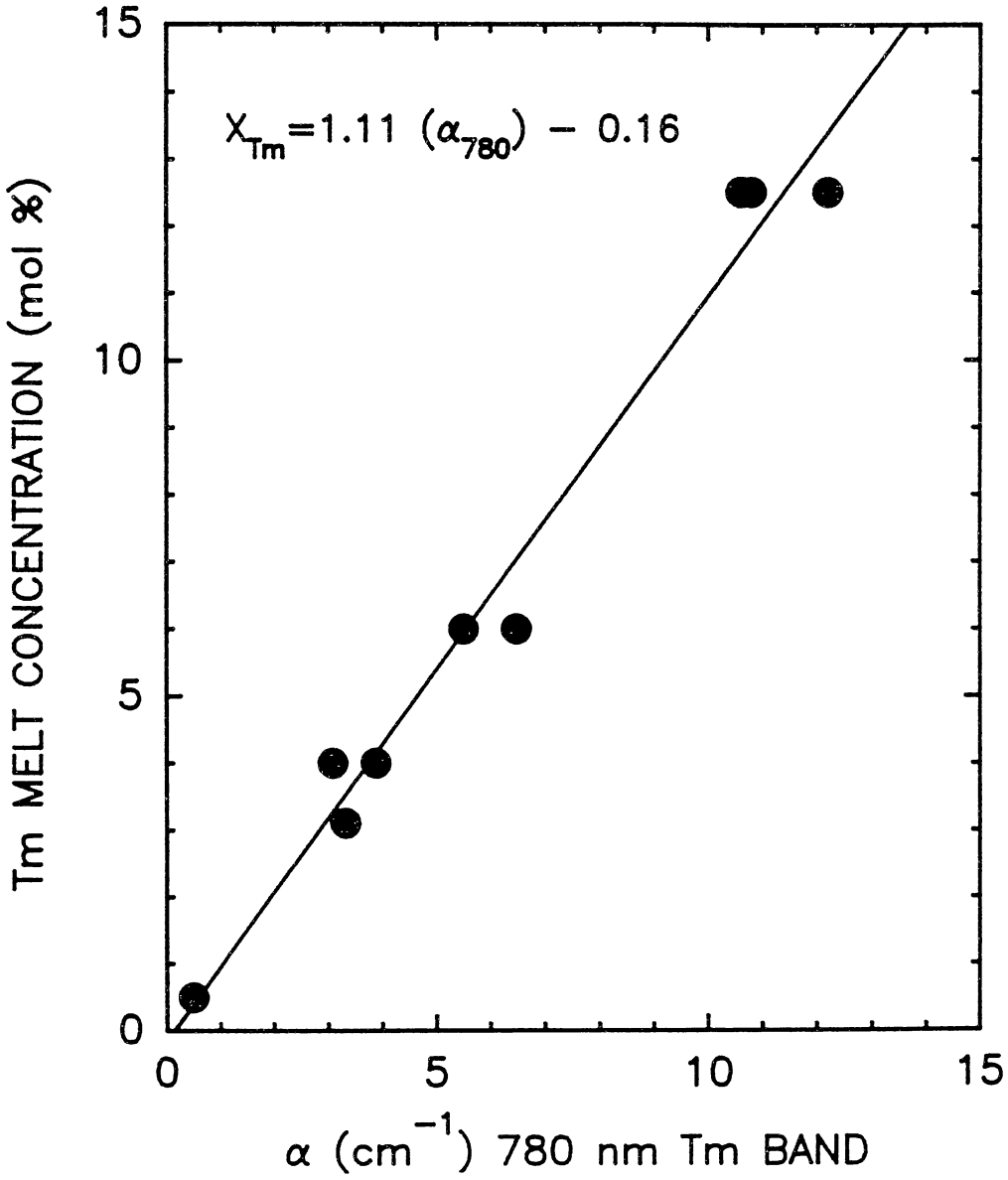


Figure 9. Thulium Concentration as a Function of the Absorption Coefficient of the 637 nm Thulium Absorption Band

The lasing characteristics of the rare earth doped crystals were investigated for possible use as efficient mid-infrared lasers. A crystal doubly doped with thulium and holmium was found to lase at about 2.07 microns with a slope efficiency of 4.92%.[7]

In summary, undoped and rare earth doped YLF crystals were grown at a rate of 1.5 mm/hr with a temperature gradient of 50°C/cm at the melting point. These crystals appeared to be uniform in the dopant concentration. The relative ease which these crystals were grown, made the Bridgman technique the preferred method by which to obtain good optical quality, research sized samples. As mentioned earlier, with the growth parameters given above, crystals were grown with this technique with nearly 100% yield.

# CHAPTER IV

# RADIATION INDUCED DEFECTS OF LITHIUM YTTRIUM FLUORIDE

## Introduction

In recent years the use of fluoride laser host materials, in particular lithium yttrium fluoride, has brought about the necessity to determine the nature of absorption bands induced by incident high energy radiation. A typical laser material is irradiated (pumped) with monochromatic light to induce the electronic transitions which lead to lasing behavior. When subjected to an environment in which incident irradiation will produce defects in the material, absorption bands related to the radiation-induced defects may appear at or near the pumping wavelength or lasing wavelength. The result may be a lowering of lasing efficiency or a stopping of lasing altogether.

In polar crystals, particularly the alkali-halides, incident radiation causes a coloration of clear and colorless crystals. This coloration is due to a radiation-induced defect which absorbs light in the visible region of the spectrum that is called a color or F-center. The accepted model for this center was proposed by De Boer in

1937[8] and consists of a halogen vacancy which has trapped an electron. The F-center is perhaps the most widely investigated, hence the best understood, point defect of all defects in ionic crystals, as the quantity and quality of literature on the subject can attest.

The formation of F-centers can be achieved a number of ways and the theory on the subject of radiation damage has been covered in great detail for general and ionic crystals.[9,10,11,12] Basically, radiation damage processes can be classified as electronic processes, elastic collisions, and radiolysis. The electronic processes include "all those in which an electronic state is changed or charge is moved about by the absorption of radiant energy"[13]. Elastic collisions are "those in which atoms or ions are displaced due to momentum and energy transfer from irradiating particles"[13] and radiolysis processes are "those in which atomic or ionic defects are produced by a series of reactions beginning with an electronic excitation."[13]

Electron irradiation was the process of F-center formation used in this study and this method falls under all three categories. However, as reported by Crawford[14] when alkali-halide crystals are irradiated with electrons, many defects are produced per incident electron than can be accounted for in a strictly elastic collision process. Though this process does indeed occur, the dominant process starts with the electronic process.

The current model for F-center production was proposed by Pooley[15] and Hersh[16] and follows the radiolysis process. The model takes into account two experimental observations. The first was the luminescence seen when the alkali-halides were irradiated with UV light and X-rays to produce the F-centers and the second was the formation of the F-center itself.

Essentially the model consists of the formation of an electronic defect called the $V_k$ or self-trapped hole center (other notation: $X_2^-$,[16] $[X_2^-]$[13]) followed by the dissociation of this center to form the F-center. The first step in the formation of this center is the creation of an electron-hole pair via an electronic process. The $V_k$ center, "discovered" by Castner and Kansig[17] using electron spin resonance (ESR) techniques, is then created when a bond is formed between two neighboring halides which in turn produces a local distortion in the lattice, the "self trapping" process.

The model proposes that the electron loses energy through either a radiative transition, hence the luminescence seen during UV and X-ray irradiation of the alkali-halides, or a non-radiative transition in a recombination event at the $V_k$ center. The end result is a relaxation of the two halides into their normal lattice sites or the formation of a vacancy with a trapped electron, the F-center, and an interstitial atom. The latter has been described as due to the relaxation of the

lattice after the recombination event and it is believed that this relaxation imparts enough kinetic energy to the alkali atom or ion to move it to an interstitial position.[15,16]

That the luminescence and F-center formation were correlated was shown in UV and X-ray irradiation of KI.[11] When irradiated at temperatures below 90 K the intensity of the luminescence was high while F-center formation was low. When irradiated above 120 K, the luminescence was low and F-center formation was high. At the intermediate temperatures a transition was observed between the luminescence and F-center formation. The disorientation temperature of KI, the temperature at which the $V_k$ center is highly mobile and unstable, is 90 K.[18,13] Direct correlation between this temperature and the onset of F-center formation served as further proof that the $V_k$ center is the direct predecessor of the F-center.

Neglecting dislocations, impurities, "as-grown" and induced Schottky and Frenkel defects, the principle radiation-induced defects introduced into ionic crystals under room temperature irradiation are $V_k$, F, F-aggregate, and interstitial aggregate centers. Of these four, only the F and F-aggregate centers exhibit strong absorption at high temperatures.

The F-aggregates are those comprised of neighboring F-centers. Using the designations presented by Sonder and Sibley,[13] a center composed of two neighboring F-centers is

designated as an $F_2$ or M-center, whereas three neighboring F-centers are designated as $F_3$ or R-centers.

In their study of the low temperature radiation effects in lithium yttrium fluoride (YLF), Renfro, et. al.[19] identified the $V_k$ center and an absorption band located at 3.99 eV, which was correlated to the time decay of the ESR signal from the $V_k$ center. The $V_k$ centers annealed between 77 and 120 K when the sample was irradiated at 10 K. After irradiation at 77 K, they observed a pink after-glow which lasted approximately thirty minutes and a decay in the ESR signal with a 1/e time of 56 minutes. They also observed a stability in the ESR signal from the $V_k$ center up to a temperature of about 200 K after a 77 K irradiation. Presumably the stability at the high temperatures is related to the time decay of the ESR signal and is an indication of electron trapping at impurity sites.

Upon electron irradiation of undoped and rare-earth doped lithium yttrium fluoride at 77 K, Renfro, et. al. also reported several polarized radiation-induced absorption bands in the UV-visible region of the spectrum. Observing the characteristics of a band centered about 3.7 eV, they identified this band as due to the F-center. Defects related to other absorption bands were not identified.

The aim of this project is to identify the radiation-induced defects which give rise to absorption bands in

lithium yttrium fluoride. This is done by using optical relations which correlate the absorption coefficients of bands seen in the absorption spectrum to that of the 3.7 eV F-center band. The half-widths at various temperatures of the 3.7 eV F-center band and a band associated with the M-center will be presented.

## Optical Relationships Between the F and F-aggregate Centers

As mentioned earlier the F-aggregate centers are comprised of neighboring F-center defects. The M-center or $F_2$ center is comprised of two neighboring F-centers and the R or $F_2$ center is comprised of three neighboring F-centers. Though other aggregate centers of higher order exhibit absorption in the same region of the optical spectrum as the F, M, and R centers, the discussion will be limited to these particular centers.

Under ionizing radiation an increasing F-center concentration results in the formation of and increase in the concentration of the aggregate centers. Under the same ionizing radiation the creation of F-centers results in the destruction of the centers by increasing the number of interstitial halogen atoms which recombine at the defects to form a normal lattice ion.

Under ionizing radiation the creation of F-centers may be written as

$$H^- + \text{"ionizing radiation"} \longrightarrow F + H^\circ, \qquad (1)$$

and the formation of M and R centers may be written as

$$F + F \Longleftrightarrow M \tag{2}$$

and

$$M + F \Longleftrightarrow R. \tag{3}$$

The reverse reactions of the above two equations is a representation of the formation of isolated F-centers concurrent with the increase of the M and R centers such that the concentration of each type of defect center increases.

Taking the case of M-center formation specifically, given a unit volume of crystal with $n_F$ F-centers and $n_M$ M-centers, the change in M-center concentration $dn_M$ upon increasing F-center concentration $dn_F$ is given by[20]

$$dn_M = (Kn_F/N)\ dn_F. \tag{4}$$

K is the number of halogen ion sites surrounding a given F-center and N the total number of halogen ion sites per unit volume of crystal. The fraction $Kn_F/N$ represents the fraction of $dn_F$ F-centers which contribute to the production of $dn_M$ M-centers. Upon integration a relation between the concentration of defects is obtained:

$$n_M = (K/2N)\ n_F{}^2. \tag{5}$$

Written in terms of concentration, Equation (5) allows use of a relation which equates the concentration of defects to the optical absorption band(s) they exhibit. This relation, known as Smakula's equation,[21] relates the concentration of the centers which give rise to a particular optical absorption band to the oscillator strength of the defect and the "shape" of the band. With

"n" the concentration of absorbing centers ($cm^{-3}$) and "f" the oscillator strength, then for a Gaussian shaped band Smakula's equation is

$$n\ f = 8.7 \times 10^{16} \frac{\mu}{(\mu^2+2)^2} W\ \alpha_{max}. \qquad (6)$$

Where W (eV) is the width at half-maximum of the band (half-width), $\alpha_{max}$ ($cm^{-1}$) is the absorption coefficient at the peak of the absorption band and $\mu$ is the index of refraction.

The significance of Smakula's equation is that, if the oscillator strength is known, the concentration of the defect which gives rise to an absorption band can be calculated directly from the optical absorption curve. As will be shown later in the configuration coordinate model of the F-center, the half-width is constant at a constant temperature. If the optical absorption spectrum is measured at constant temperature Smakula's equation may be written

$$n = (\text{constant})\ \alpha_{max}. \qquad (7)$$

With this relation Equation (5) may be rewritten as

$$[\alpha_{max}]_M = D\ [\alpha_{max}]_F^2. \qquad (8)$$

Where the constant D is

$$D = 8.7 \times 10^{16} \frac{K}{2N} \frac{C_F^2}{C_M} \frac{W_F^2}{W_M} \frac{f_M}{f_F^2} \qquad (9)$$

and $C_i = \mu/(\mu^2+2)^2$. In a like manner for the R-center equilibrium, the relation is

$$[\alpha_{max}]_R = (\text{constant})\ [\alpha_{max}]_F^3. \qquad (10)$$

The relations given by Equations (8) and (10) are

valid only under increasing F-center production. Eventually the recombination process represented by

$$F + H^{\circ} \longrightarrow H^{-}, \qquad (11)$$

increases to a point at which there is no net increase in the concentrations of the F and F-aggregate centers. Only at concentrations below this point, termed the saturation point, can the relations be verified.

The quadratic and cubic relationships represented by Equations (8) and (9) have been confirmed for the NaCl structured alkali-halides at radiation temperatures ranging from liquid helium to room temperatures.[22,23,24] The quadratic relationship has also been shown to hold true for the M-center in $KMgF_3$.[25] The two relations then provide a method of associating absorption bands to the centers from which they arise if an absorption band due to the F-center is known. After successive irradiation at a fixed temperature, measurement of the peak absorption coefficient of each band can be correlated with that of the F-center band. Hence a plot of $\log[\alpha_{center}]$ versus $\log[\alpha_F]$ will yield a straight line whose slope will attribute a particular band to a particular defect. A band due to the M-center will yield a slope of 2 and a band due to the R-center will yield a slope of 3. In the case in which the F-center exhibits more than one absorption band then the slope of the line on the log-log plot will equal 1.

The question on the number of bands which might be associated with a particular defect may be qualitatively

answered by the simple model of a particle in a box. For this model the energy eigenvalues are given by

$$E = \frac{h^2}{8m^2} \left[\frac{n_1^2}{a^2} + \frac{n_2^2}{b^2} + \frac{n_3^2}{c^2}\right]. \qquad (12)$$

where h is Planck's constant, m is the mass of the electron, a,b, and c are the dimensions of the box and $n_1$, $n_2$, and $n_3$ are the quantum numbers for each degree of freedom. For a cubic box, a = b = c and the energy between the ground state ($n_1 = n_2 = n_3 = 1$) and the first excited state ($n_1 = 2$, $n_2 = n_3 = 1$) is given by

$$E_{211} - E_{111} = \frac{3h^2}{8ma^2}. \qquad (13)$$

The energy is single valued in the transition from the ground state to the first excited state in the case of a cubic box. In the alkali-halides such a transition is seen in the optical absorption spectrum. Only one band is associated with a transition to the first excited state.

In the NaCl structured alkali-halides the M-center lies along [110] and corresponds to the case in which $a \neq b \neq c$. Hence there are three possible orientations for the dipoles associated with this defect: along the axis of the center [110], and the two perpendicular to the center [001] and [1$\bar{1}$0]. For light polarized along the axis of the center the absorbance lies to the low energy side of the F-center and gives rise to the most prominent absorption band associated with the M-center. For light polarized perpendicular to the axis of the M-center the absorbance is weak and has been found to lie underneath the strong F-

center absorption band.[13,26,27]

In scheelite structured lithium yttrium fluoride, the fluorine anion has as its first nearest neighbor a lithium ion at a distance of roughly 0.33a (a = 5.16Å)[28], a next nearest neighbor yttrium ion at roughly 0.46a and another yttrium ion at roughly 0.47a. Lacking the symmetry of the NaCl structure in which the anion has six equidistant nearest neighbors, it is expected that there are three absorption bands associated with the F-center in lithium yttrium fluoride. In the case on the M-center in lithium yttrium fluoride, it is expected that there is one prominent band; the band which is associated with the dipole transition along the axis of the defect.

## The Configuration Coordinate Model: Width of the F-center Absorption Band

In the adiabatic or Born-Oppenheimer approximation[29] the crystal Hamiltonian may be separated into two parts. One dealing with the electronic displacements and the other dealing with the nuclear displacements. The two parts are coupled by the electronic energy eigenvalues which act as an effective potential of the nuclear equation. Hence the electronic states are determined by the nuclear coordinates and the nuclear coordinates are determined by the average positions of the electrons.

With $\bar{r}$ and $\bar{R}$ representing the electronic and nuclear coordinates respectively, the wavefunction $\Psi$, which is the

solution to the crystal Hamiltonian, may be written by the product

$$\Psi(\bar{r},\bar{R}) = \phi_{n,\bar{R}}(\bar{r}\rangle\ \chi_{nN}(\bar{r},\bar{R}). \tag{14}$$

Here n and N are the electronic and nuclear quantum numbers, $\phi_{n,\bar{R}}(\bar{r})$ is the electronic wavefunction which depends parametrically on $\bar{R}$, $\chi_{nN}(\bar{R})$ is the nuclear wavefunction which is dependent on the electronic quantum numbers.[26] Separately the electron and nuclear wavefunctions satisfy

$$[T_e + U(\bar{r},\bar{R})]\ \phi_n(\bar{r},\bar{R}) = E_n(\bar{R})\ \phi_n(\bar{r},\bar{R}) \tag{15}$$

$$[T_N + V_n(\bar{R})]\ \chi_{nN}(\bar{r},\bar{R}) = E\ \chi_{nN}(\bar{r},\bar{R}). \tag{16}$$

The T's represent the electronic (e) and nuclear (N) kinetic energies and $U(\bar{r},\bar{R})$ represents electron potential energy when the nuclei are displaced from their equilibrium positions. $V_n(\bar{R})$ is the sum of the electronic energy eigenvalues and a potential energy term for the displacement $\bar{R}$ of the nuclei equilibrium.[26,30]

The probability of an optical transition at the color center is given by the square of the dipole matrix element $\langle\Psi_e|\bar{r}|\Psi_g\rangle$ connecting the two electronic states. Hence, the dipole matrix element $\bar{r}$ is given by[30]

$$\bar{r}_{eg} = \langle\phi_{k\bar{R}}(\bar{r})|\bar{r}|\phi_{n\bar{R}}(\bar{r})\rangle\ \langle\chi_{kN}(\bar{R})|\chi_{nN}(\bar{R})\rangle. \tag{17}$$

The first term is the electronic dipole moment and is related to the probability of the n to k transition. The second term is typically called the vibrational overlap integral and determines the optical lineshape of the absorbing center. In the harmonic approximation the

potential $V_n(\bar{R})$ is expanded in a Taylor series to second order in the displacements $\bar{R}$ of the nuclei about their equilibrium positions. The set of functions $\chi_{nN}(\bar{r},\bar{R})$ are then the quantum mechanical harmonic oscillator wavefunctions.

In the single-mode or linear coupling model the ground and excited states are assumed to be coupled to a single vibrational mode. With this simplification the system can be represented by using a single normal coordinate Q. In the harmonic approximation the potentials of both the ground and excited states are represented by parabolas. In Figure 10 these potentials are plotted versus the configuration coordinate Q. The ground state is represented by the curve $E_g$ and the excited state is represented by the curve $E_e$. The minima of the ground state is defined as q=0 and the excited state has a minima that is shifted by the value $q_o$. At T=0 the lowest energy levels of the ground state are occupied. With n=0 the quantum mechanical solution of the harmonic oscillator problem gives a Gaussian in the probability amplitude which is centered about q=0. According to the Franck-Condon approximation the neighboring ions do not move during an electronic transition. During optical absorption, say from the n=0 energy level, the transition is vertical. With the electron in the excited state, say at k=2, the average positions of the electrons relative to the ground state has changed and the ions shift their positions to the new

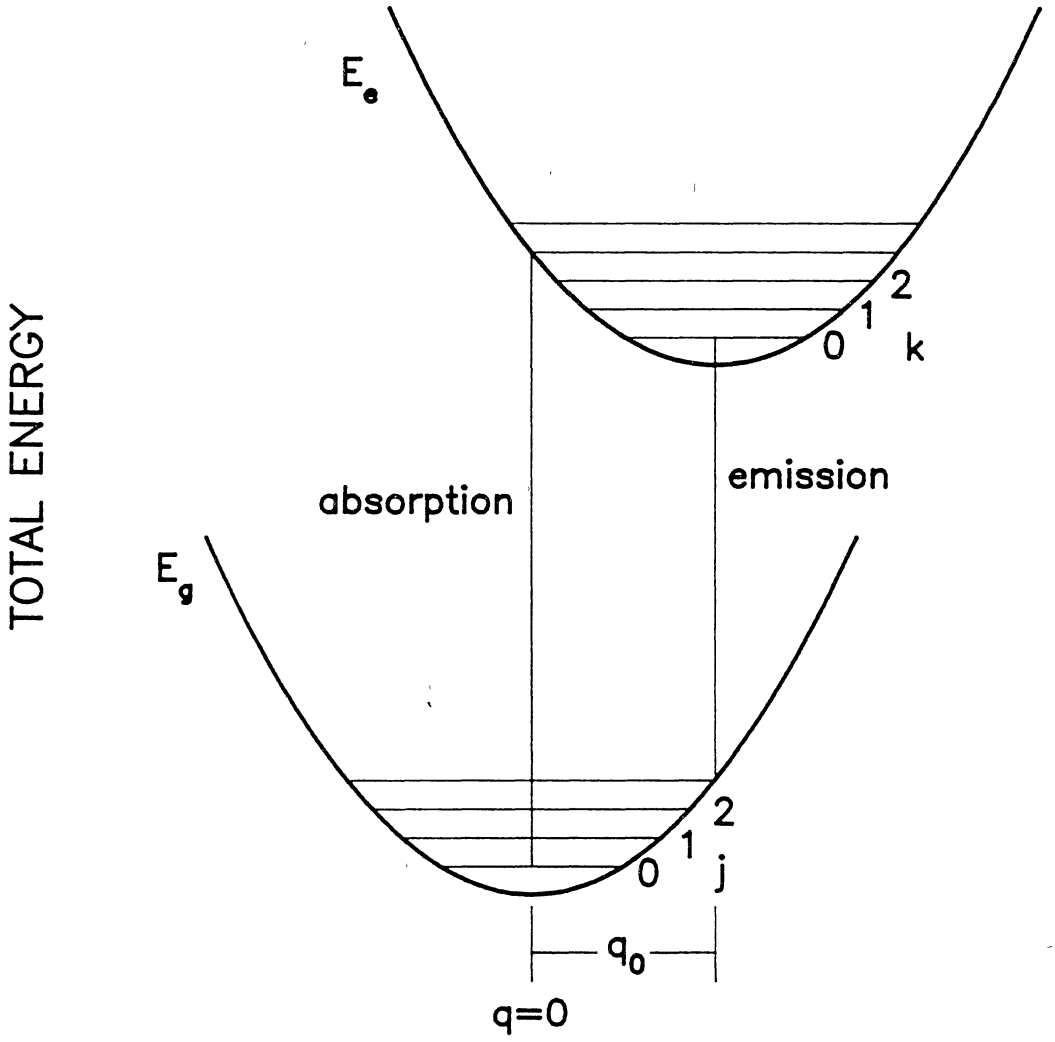


Figure 10. Configuration Coordinate Diagram

equilibrium value of $Q=q_o$. Concurrent with the shift is a loss in electron energy during a nonradiative transition to the k=0 level. From the k=0 level the electron then loses energy via a radiative transition to the ground state.

For linear coupling the frequency in each state remains the same and the ground state energies are given as[32]

$$\epsilon_{gn} = (n + 1/2)\ \hbar\omega \tag{18}$$

and the excited states energies are given as

$$\epsilon_{ek} = (k + 1/2)\ \hbar\omega + E_{ge} - S\hbar\omega. \tag{19}$$

$E_{ge}$ is the difference in energy between the ground state and the excited state potentials at q=0 when T=0. M is the effective mass of the mode and S is a dimensionless constant which measures the strength of the coupling which shifts the equilibrium position of the excited state relative to the ground state[30] and is called the Huang-Rhys factor.[33]

Evaluation of the vibrational overlap integral gives for the normalized transition probability,[30,32]

$$W_{kn} = \exp(-S)\ (k!/n!)\ S^{n-k}\ [L_m^{n-k}(S)]^2 \tag{20}$$

where the L's are Laguerre polynomials. At T=0, n=0, and the probability for a transition to the $k^{th}$ level is

$$W_{k0} = (S^k/k!)\ \exp(-S). \tag{21}$$

The absorption spectrum consists of a series of lines at $E_k = E_{eg}-S\hbar\omega+k\hbar\omega$ peaked at $n\simeq S$ and weighed in intensity by $W_{k0}$. From this and the energy equation for the excited state, S is the energy difference between the most probable

transition $E_{eg}$ and the lowest energy level of the excited state. In this respect S is the number of phonons created in the transition to the excited state.

In his analysis of the absorption, Markham[31] gives the width at half-maximum or half-width as a function of temperature as

$$W(T)^2 = W(0)^2 \coth(h\nu/2kT). \qquad (22)$$

Here W(T) is the half-width and $\nu$ is the frequency of the mode which is assumed to interact with the defect. T is the absolute temperature and k is Boltzmann's constant. W(0) is the half-width at T=0 and is given by

$$W(0)^2 = (8\ln 2)\ (h\nu)^2\ S. \qquad (23)$$

From Equation 22, the half-width at low temperatures is relatively constant and a low temperature value of the half-width may be used as an approximation of W(0). With W(T) obtained at various temperatures, the frequency $\nu$ may be obtained by plotting in a plot of $\coth^{-1}[(W(T)/W(0))^2]$ versus 1/T. This should yield a straight line which passes through the origin and has a slope of $h\nu/2k$. The value of $\nu$ obtained from the slope may then be used to calculate the Huang-Rhys factor S using the expression for W(0).

The analysis of the configuration coordinate diagram leads to a single value of the vibrational frequency interacting with the center, but should be viewed as an average frequency since there is a large distribution of vibrational modes in a crystal. In KCl the effective frequency obtained is $2.96 \times 10^{12}$ Hz and the longitudinal

optical frequency is $6.4 \times 10^{12}$ Hz.[34] For the NaCl the effective frequency is $4.4 \times 10^{12}$ Hz and longitudinal optical frequency $8.1 \times 10^{12}$ Hz.[34] Hence the effective frequency may be considered as the average frequency obtained in which the interaction of the defect is limited to the nearest neighbors and not the lattice modes of the pure crystal.

# CHAPTER V

## EXPERIMENTAL PROCEDURE

The lithium yttrium fluoride samples were obtained from an undoped single crystal which was grown using the Czochralski technique. The crystal, grown along [100] of the tetragonal unit cell, had a slightly elliptical cross section perpendicular to the growth direction. A simple conoscope, similar to that described by Bond,[35] indicated that the optic axis lies along the semi-major axis of the ellipse. This result is in agreement with Uhrin and Belt[3] for YLF crystals grown along [100]. A cross sectional slice was then cut from the boule using a diamond saw, and oriented using a back-reflection X-ray Laue. Each sample was then cut with a flat indicating the c-axis, or [001], and with an a-axis ([100] or [010]) perpendicular to the optic faces.

The samples were rough polished using 600 grit silicon carbide powder then polished to an optical finish using 12 micron polishing films with isopropyl alcohol as a lubricant. It was found that some polishing fluids and lubricants, such as the water based cerium oxide polishing compound and the water based extenders for diamond pastes as well as mineral oil as a lubricant on the polishing

films, had a tendency to etch or pit the surfaces of the sample. The final thickness of each sample was about 2 millimeters.

A Perkin Elmer 330 spectrophotometer, interfaced with a computer, was used to measure the absorbance or optical density from 800 to 200 nanometers. Absorption due to radiation-induced defects was not found in the 800 to 2500 nanometer range. The data were recorded in increments of 1 nanometer with calcite polarizers placed in the sample and reference beams. With the assumption that the reflectivity did not change upon the introduction of F and F-aggregate centers, the absorption coefficient $\alpha$ was calculated using the expression

$$\alpha = \frac{23.03 \log[\text{optical density}]}{t(\text{mm})} \quad (\text{cm}^{-1}) \qquad (25)$$

In this expression t is the thickness of the sample in millimeters.

Absorbance measurements were taken after electron irradiation at room temperature (300 K) or dry ice temperature (195 K). These measurements were done at liquid nitrogen temperature (77 K) with the sample mounted in a vacuum sealed cryostat. Mounted in the cryostat, the sample is sandwiched between the copper cold finger of the cryostat and a copper flange. Thermal contact between the sample and the cold finger was aided by a thin layer of low temperature thermal compound. The temperature of the sample was read with a type K (chromel-alumel) thermocouple mounted on the cold finger next to the sample.

The cryostat is designed with a rotary seal so that the mounted sample can be aligned with a pair of silica windows for absorbance measurements or silica and aluminum (5 thousandths inch thickness) windows for irradiation purposes. The cryostat was evacuated before each data set using a high vacuum pumping system. The final internal pressure attained was on the order of $10^{-6}$ Torr.

The absorbance was also measured at temperatures ranging from 9 K to 300 K in order to measure the temperature dependence of the half-widths of the F and M-center absorption bands. This was done by mounting the sample on the cold head of a TRI Research T2000 closed cycle helium refrigerator. The view ports on the cold head cover were also made of silica and contact between the cold finger and the sample was aided by the use of a low temperature thermal compound. The temperature was monitored with a CTI Cryogenics temperature controller using a silicon diode for temperature measurement. The controller also supplied power to a manganin wire heater. Deviation between set point and measured temperature was not apparent below 80 K. At higher temperatures, above ≈140 K, the temperature oscillated ±8 K.

The electron irradiations were performed at both 300 and 195 K using 1.75 MeV electrons from a Van de Graaff electrostatic accelerator. Dry ice temperature was attained with dry ice and acetone as a heat exchange medium. It was expected that irradiation at this

relatively low temperature would cause a large increase in the temperature of the sample. Consequently, when long irradiation times were desired, the beam current was pulsed in increments of not longer than 5 seconds after which a minute was allowed to elapse before the next current pulse. After irradiation the dry ice-acetone solution was removed and air was blown into the dewar cavity to remove excess acetone. Liquid nitrogen was then added to cool the sample for absorbance measurements.

The beam current was passed through the aluminum window of the cryostat and the current density was measured at about 2 microA/$cm^2$. This current density corresponds to a maximum dose rate of $1.09 \times 10^{14}$ MeV/$cm^3$/sec for a sample 2 millimeters thick. This dose rate may be high since the penetration depth of the electrons was not actually measured. After each irradiation the YLF samples exhibited a bluish emission. This emission decayed within 5 minutes when the sample was irradiated at 300 K and within 10 minutes when irradiated at 195 K.

# CHAPTER VI

## RESULTS AND DISCUSSION

In a previous study on the $[F_2^-]$ or $V_k$ center in undoped and rare-earth doped YLF, Renfro, et. al.[19] reported five polarized radiation-induced absorption bands after electron irradiation at 77 K. Two of these bands, which at 77 K are located at 3.02 and 3.7 eV (410 and 335 nm), were strongly polarized parallel to the c-axis and the other three bands, which at 77 K are located at 2.29, 2.88, and 3.7 eV (540, 430, and 335 nm, respectively), were strongly polarized perpendicular to the c-axis. Comparing the absorbance spectra of undoped and rare-earth doped YLF, they observed that the characteristics (position, half-width, and polarization) of the 3.7 eV band did not vary. They identified this band as due to the F-center. Defects associated with the other bands was not reported.

The absorption coefficient of unirradiated and irradiated YLF, measured at 77 K, versus photon energy is shown in Figure 11. The lower solid curve is the polarized ($\vec{E}_{\perp}c$) background absorption of YLF. This curve is identical to the $\vec{E}\|c$ background curve and is of a sample that had been previously irradiated and annealed. This curve also matches the background absorption of the as-

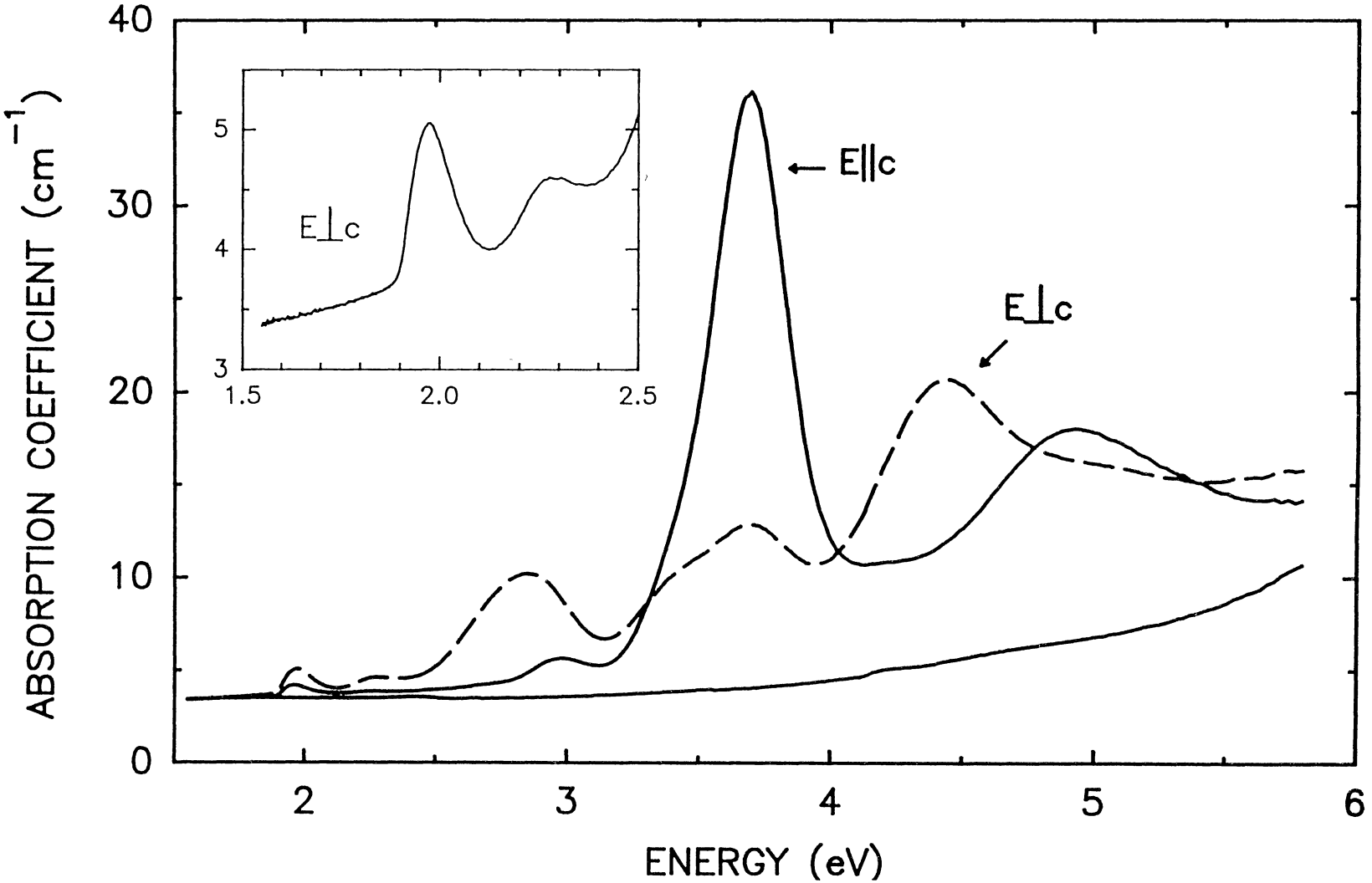


Figure 11. Polarized Optical Absorption Spectra of Unirradiated and Electron Irradiated Lithium Yttrium Fluoride

received sample. The unpolarized absorption of unirradiated YLF (not shown) is relatively flat over the energy range shown. Consequently, the increase in the background absorbance at energies greater than 3 eV is an artifact of the calcite polarizers.

After a 10 second room temperature irradiation, a dose of about $1.08 \times 10^{15}$ MeV/cm$^3$, YLF exhibits several absorption bands as shown in the top two curves in Figure 11. The upper solid curve is the absorption obtained with light polarized parallel to the c-axis ($\vec{E} \| c$). At this polarization, YLF exhibits four absorption bands which, at 77 K, are located at 1.96 eV (632 nm), 2.98 eV (416 nm), 3.7 eV (335 nm), and 4.94 eV (251 nm). The $\vec{E} \perp c$ spectrum, the dashed curve of Figure 11, exhibits at least 7 bands in the same energy range. At 77 K, these bands are located at 1.97 eV (628 nm), 2.3 eV (538 nm), 2.88 eV (430 nm), 3.7 eV (334 nm), and 4.43 eV (280 nm). Also apparent are two bands which appear as shoulders to the bands at 3.7 and 4.43 eV.

The 3.7 eV band at both polarizations is the F-center band identified by Renfro, et. al. The $\vec{E} \perp c$ 1.97 eV band, not mentioned but seen in the optical spectrum presented in the earlier study, appears to be the same as the $\vec{E} \| c$ 1.96 eV band; a shift in peak position of 4 nanometers. Figure 12 shows the room temperature (300 K) absorption coefficient versus angle of these two bands. The absorbance of each band is nonzero at all polarizations, an

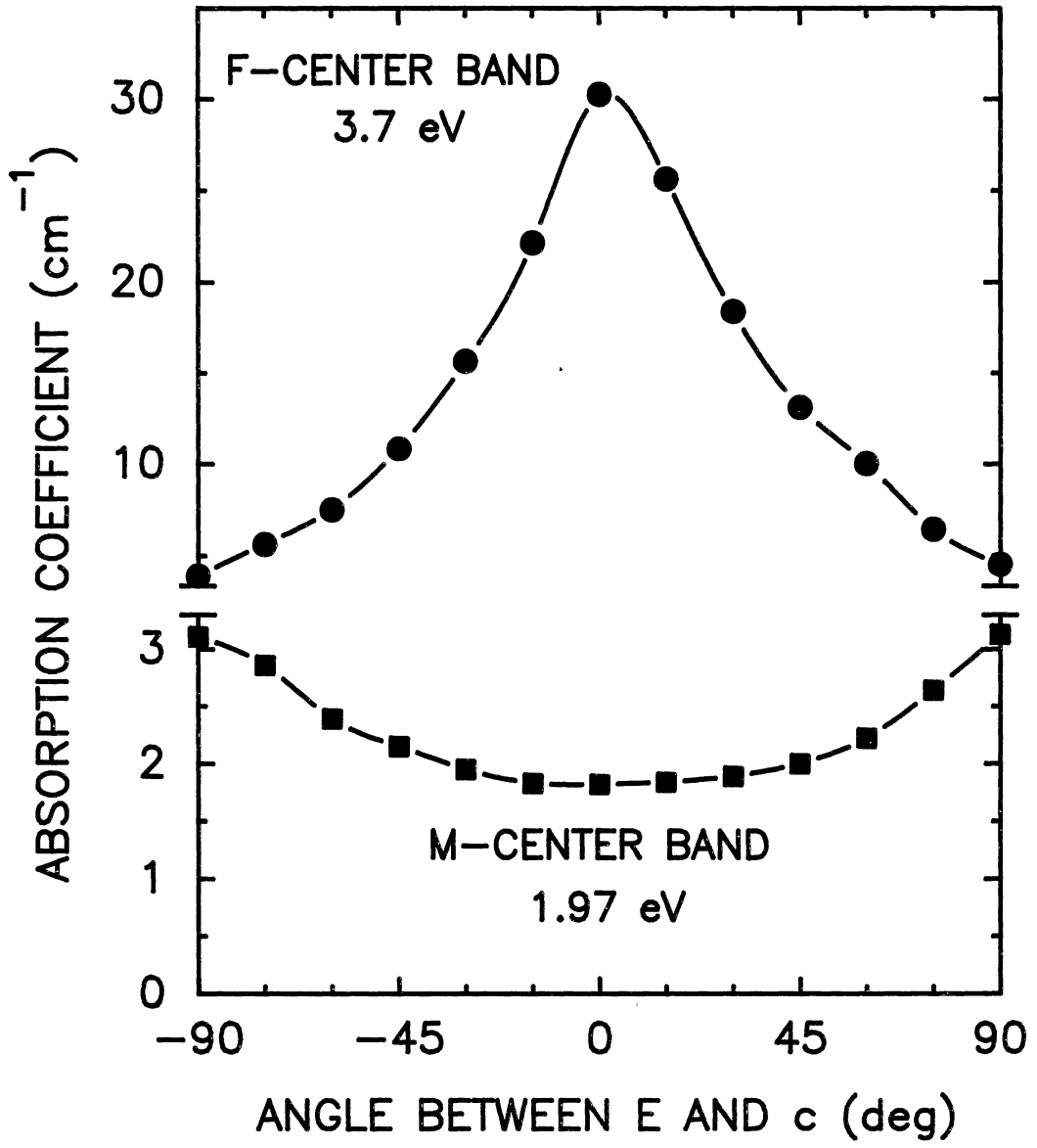


Figure 12. Maximum Optical Absorption of the 3.7 eV F-center and 1.97 eV M-center Bands as a Function of Polarization Angle

indication that each band is the average contribution of dipoles oriented at some, as yet, unknown angle to the c-axis.

The $\vec{E}\|c$ 2.98 eV band corresponds to the $\vec{E}\|c$ 3.02 eV band reported by Renfro and the three bands designated by Renfro to be polarized perpendicular to the c-axis also correspond to bands seen in Figure 11. Renfro, et. al. did not mention the 4.94 and 4.43 eV bands of Figure 11, but an examination of the spectrum they presented clearly shows the 4.43 eV band. The 4.94 eV band may have been present in their irradiated samples, but the use of Polaroid sheets to obtain the absorbance spectrum limits spectrophotometers to an energy of about 4.95 eV (250 nm). Their absorbance plots terminated at about this energy.

In subsequent plots the 2.85 and 4.43 eV bands are also labeled F-center bands, the 1.97 eV band is labeled an M-center band, and the 2.3 eV band is labeled an R-center band. The correlation of these bands to the 3.7 eV F-center band, to be presented in the latter part of this discussion, provides the basis for the designations.

Figures 13 and 14 are the production curves (absorption coefficient versus dose) of the three F-center bands and the M-center band when irradiated at room and dry ice temperatures, respectively. The 2.3 eV R-center band has been omitted in both figures since the growth structure of this band cannot be distinguished on this scale.

At the high dose rates used in this study and at each

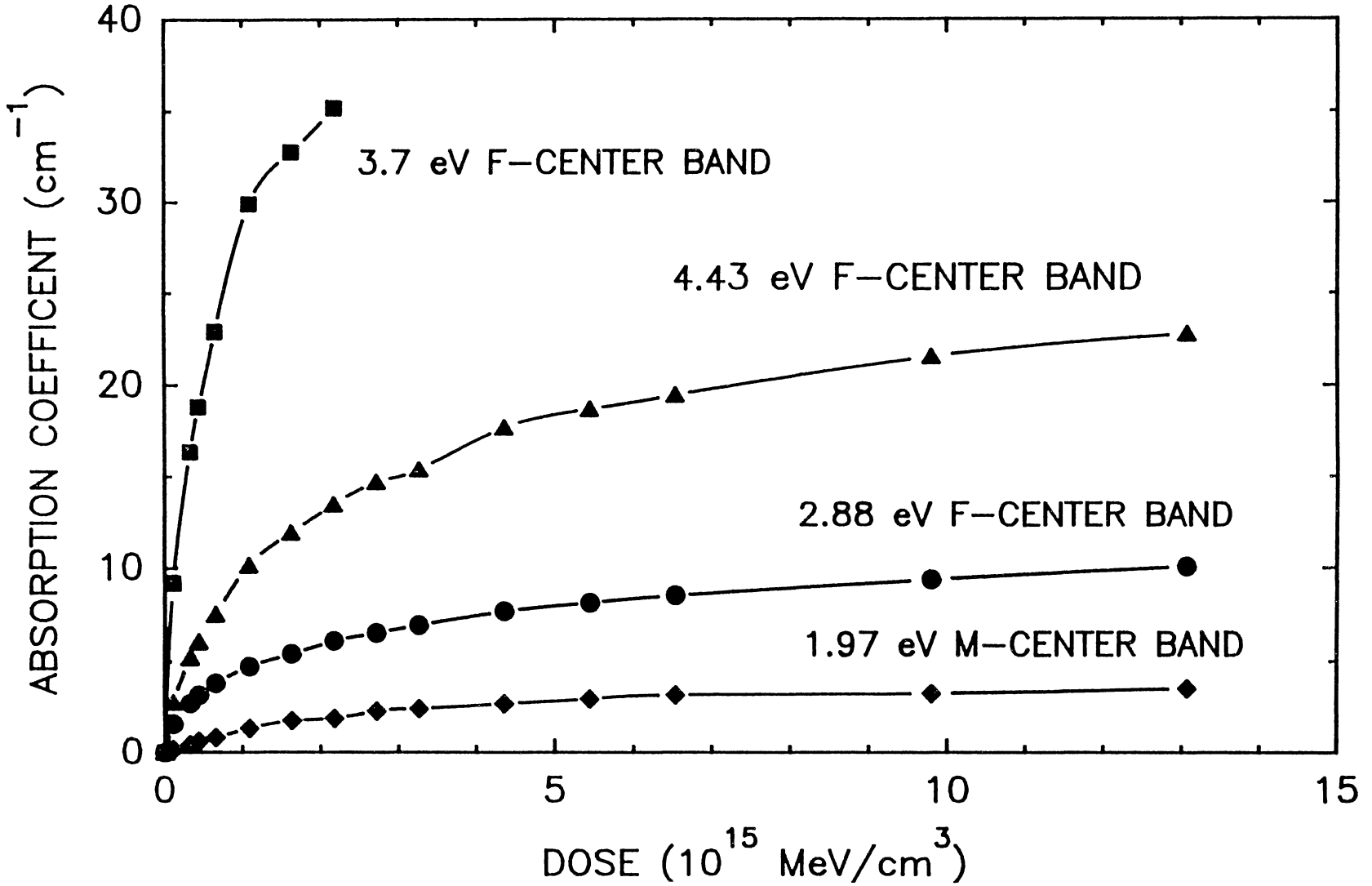


Figure 13. Production Curves of the Radiation Induced Absorption Bands at a Radiation Temperature of 300 K. Shown are the 77 K Absorption Coefficients.

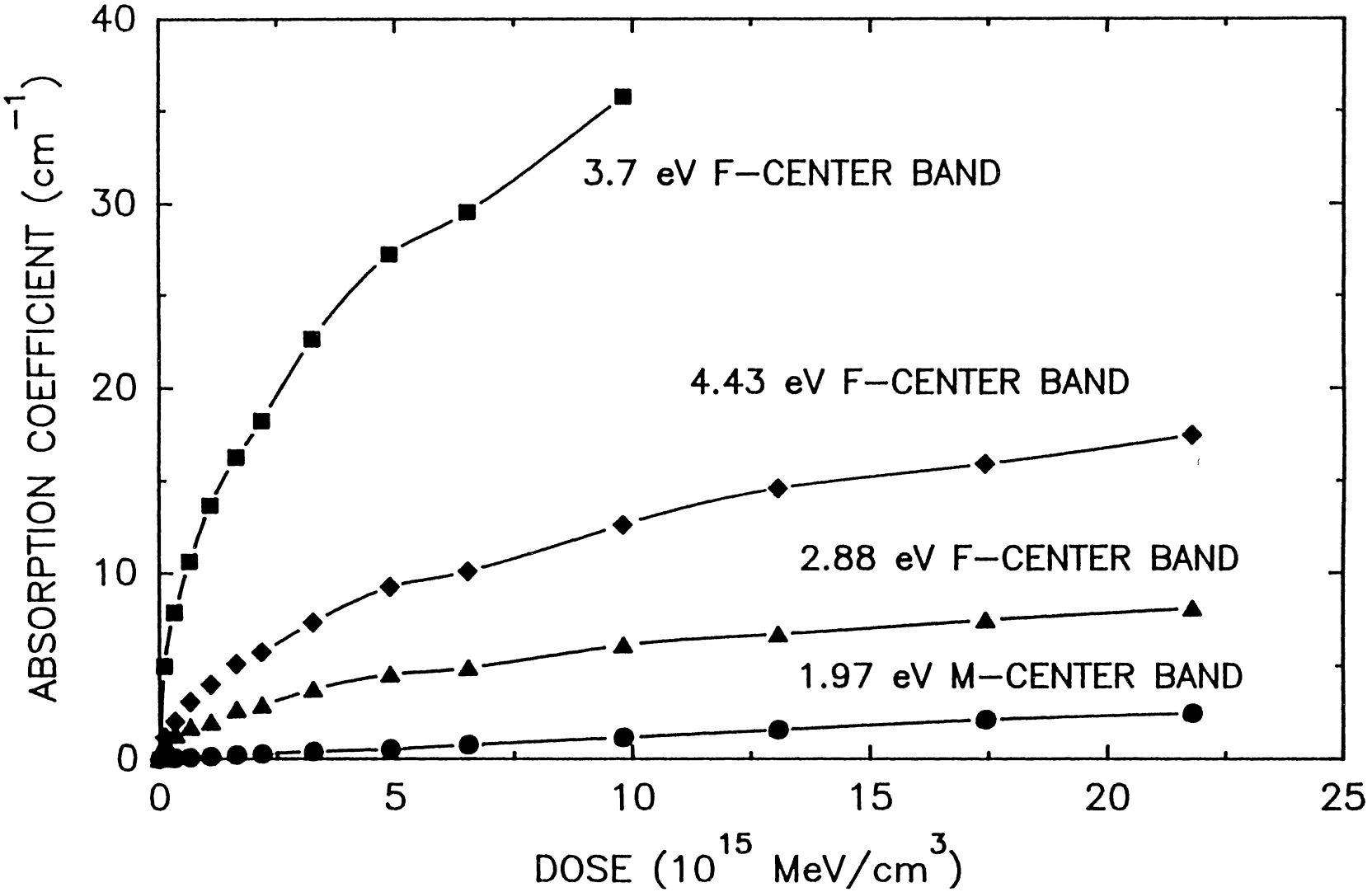


Figure 14. Production Curves of the Radiation Induced Absorption Bands at a Radiation Temperature of 195 K. Shown are the 77 K Absorption Coefficients.

temperature, the 3.7 eV F-center band reaches the maximum measurable optical density of the spectrophotometer before saturation of all the bands occurs. These growth curves show the same characteristics that are seen in the alkali-halides. The peaks show an initial fast growth at low irradiation times followed by a much slower increase until saturation of the bands is reached.

The number of data points used in correlating the absorption coefficients of the four above-mentioned bands to the 3.7 eV F-center band was limited to 7 for the room temperature irradiation data and to 9 for the 196 K irradiation data. The absorption coefficients were measured at 77 K since at this easily attainable temperature the absorption bands were clearly defined.

The growth of the $\vec{E}\perp c$ 1.97, 2.3, 2.85, and 4.43 eV bands were correlated with the growth of the $\vec{E}\parallel c$ 3.7 eV F-center band. Each correlation consisted of relating the absorption coefficient of the bands in question to that of the 3.7 eV F-center band. Thus the relation assumed was of the form

$$\alpha = C\ \alpha_F^n, \tag{26}$$

where C is a constant of proportionality and the value of n associates the absorption band with a particular defect band as discussed in the first chapter.

## The F-center in Lithium Yttrium Fluoride

From the particle in a box model for the F-center, the

number of bands expected to be associated with the F-center in lithium yttrium fluoride (YLF) is three. With the identification of the band at 3.7 eV as an F-center band, correlation of absorption coefficients can be used to identify other bands due to the F-center as discussed in the previous chapter.

At corresponding doses, the maximum absorption coefficients of the 2.88 eV band are plotted versus the maximum absorption coefficients of the 3.7 eV F-center band in Figure 15. The data plotted are the absorption coefficients obtained from the 77 K absorbance spectra after irradiation at room temperature (300 K) and dry ice temperature (195 K). These same data are shown in the production curves of Figures 11 and 12. The two lines shown in the plot are the linear regressions of the data. The slope of the line obtained for the 300 K irradiation data is 0.98 and the slope of the line for the 195 K data is 1.0.

The data plotted in Figure 16 are the maximum absorption coefficients obtained for the 4.43 eV band versus the absorption coefficients of the 3.7 eV F-center band. Again the lines are those obtained from a linear regression. The slope of the line for the 300 K irradiation data is 1.16, while slope of the line for the 195 K irradiation data is 1.21. From this we see that both bands grow linearly with the F-center. The simplest description for these bands are that they also are due to

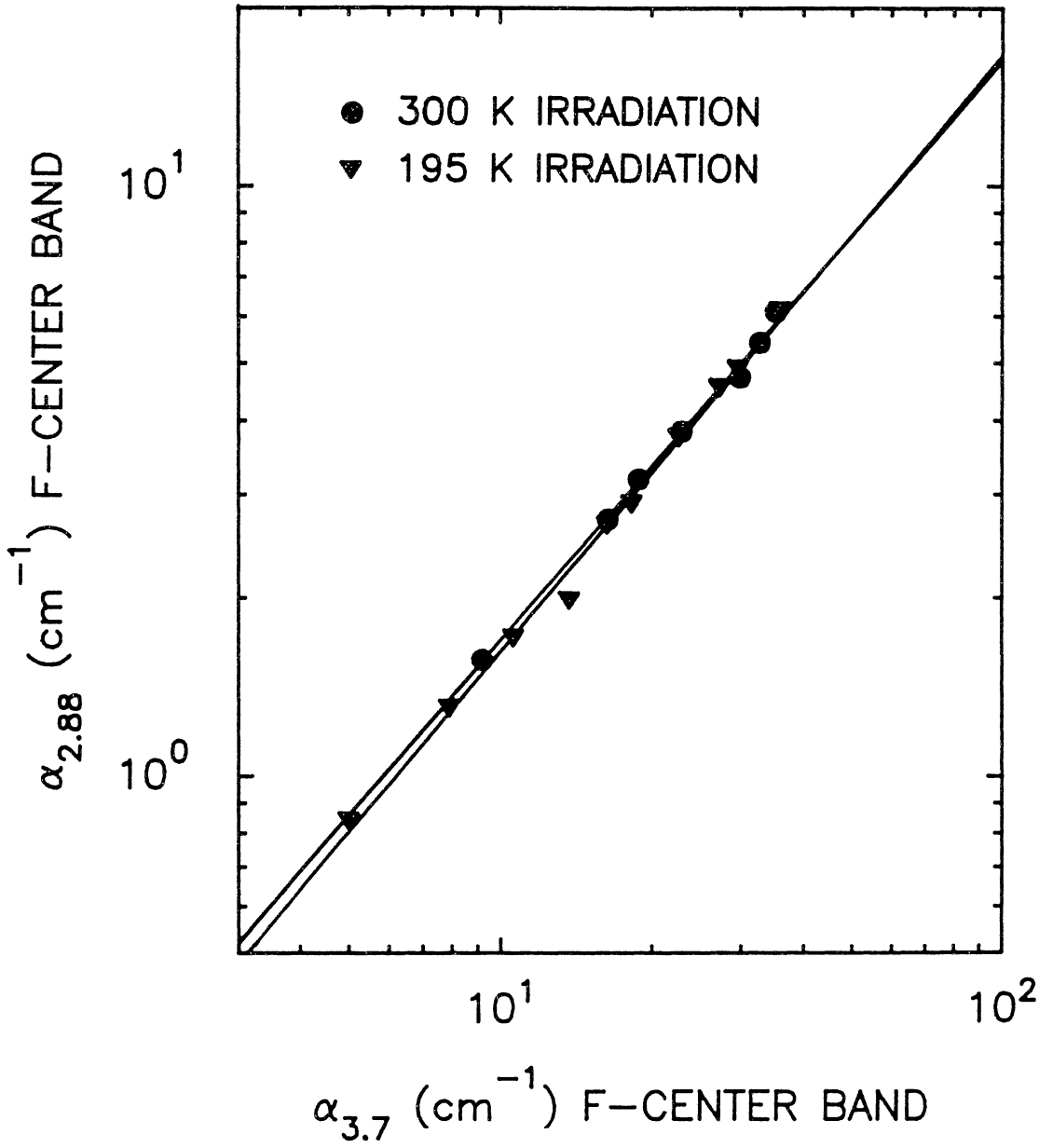


Figure 15. Absorption Coefficient of the $\vec{E}\perp c$ 2.88 eV F-center Band as a Function of the Absorption Coefficient of the $\vec{E}\parallel c$ 3.7 eV F-center Band. The Absorption Coefficients were Measured at 77 K after Irradiation at 300 K and 195 K.

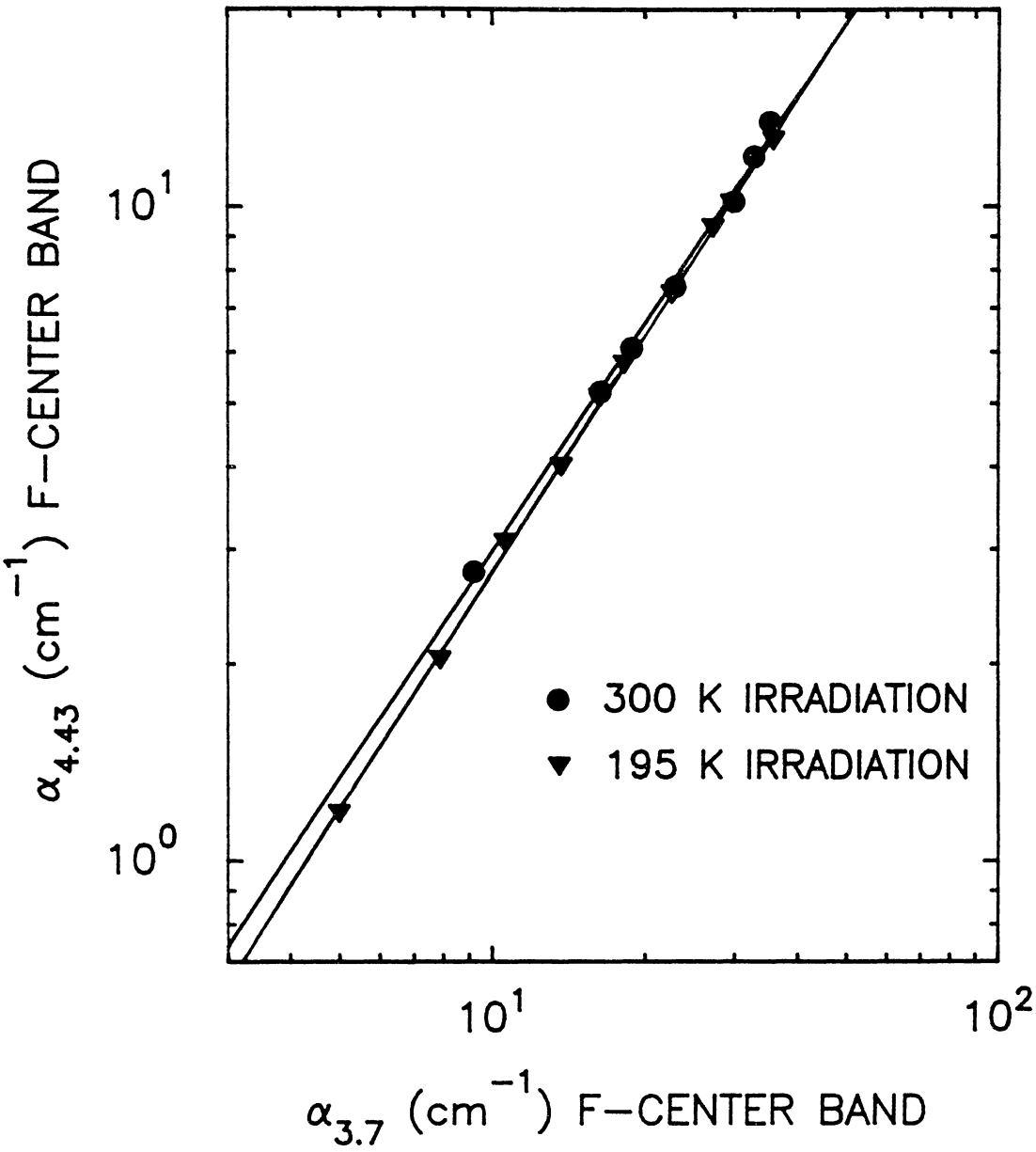


Figure 16. Absorption Coefficient of the $\vec{E}\perp c$ 4.43 eV F-center Band as a Function of the Absorption Coefficient of the $\vec{E}\parallel c$ 3.7 eV F-center Band. The Absorption Coefficients were Measured at 77 K after Irradiation at 300 K and 195 K.

the F-center.

From Figure 11, after a 1 second 300 K irradiation the 3.7 eV F-center has an absorption coefficient of 9.18 $cm^{-1}$. From Smakula's equation the minimum concentration of F-centers formed (f=1, W=0.36 eV) after the one second irradiation is about $2x10^{16}$ $cm^{-3}$. With a dose rate of $1.09x10^{14}$ $Mev/cm^3/s$ then the number of F-centers formed per incident electron is about 300. This high number indicates that the elastic collision process of defect formation does not contribute significantly to F-center formation in YLF. Hence, as has been found in other halide crystals, the radiolysis process is the principle damage mechanism.

The absorption band at 3.7 eV had previously been identified as due to the F-center and is strongly polarized parallel to the c-axis as shown in Figure 12. The $\vec{E}\|c$ maximum absorption coefficient and the width at half-maximum of this band is given at various temperatures in Table I for two different samples. The data were taken after room temperature electron irradiations to doses of $1.11x10^{15}$ $MeV/cm^3$ and $4.7x10^{14}$ $MeV/cm^3$ for the upper and lower sets of data, respectively.

From Smakula's equation, for a fixed concentration of absorbing defects the product of the maximum absorption coefficient and the half-width should remain constant at all temperatures. The data in Table I show that at least in the intermediate temperatures this product (labeled PRODUCT in Table I) remains relatively constant. This is

TABLE I

TEMPERATURE DEPENDENCE OF THE ABSORPTION COEFFICIENT AND THE WIDTH AT HALF-MAXIMUM OF THE 3.7 eV F-CENTER BAND WITH $\vec{E} \| c$

| TEMPERATURE (K) | ABSORPTION COEFFICIENT ($cm^{-1}$) | HALF-WIDTH (eV) | PRODUCT ($cm^{-1}$ eV) |
|---|---|---|---|
| 298 | 18.87 | 0.542 | 10.23 |
| 194 | 23.47 | 0.450 | 10.56 |
| 135 | 26.78 | 0.392 | 10.50 |
| 72 | 29.14 | 0.364 | 10.61 |
| 9 | 29.79 | 0.340 | 10.04 |
| 298 | 13.67 | 0.538 | 7.35 |
| 235 | 14.75 | 0.476 | 7.02 |
| 200 | 15.91 | 0.454 | 7.22 |
| 160 | 17.33 | 0.420 | 7.28 |
| 120 | 18.81 | 0.386 | 7.26 |
| 80 | 19.90 | 0.360 | 7.16 |
| 40 | 20.69 | 0.340 | 7.03 |
| 9 | 20.79 | 0.341 | 7.09 |

consistent with the results obtained for the F-centers in the alkali-halides. At low temperatures the half-width remains relatively constant up to 40 K and for comparable temperatures between the two data sets the half-width values agree to within a few percentage points.

Figure 17 shows the plot of $\coth^{-1}[W(T)^2/W(0)^2]$ versus 1000/T with W(0) taken to be the average value of the 9 K half-widths. The straight line is the least squares fit through the first eight data points or from temperatures greater than 80 K. At the lower temperatures, less than 120 K, the data deviate from the straight line and may be an indication that at these low temperatures a different

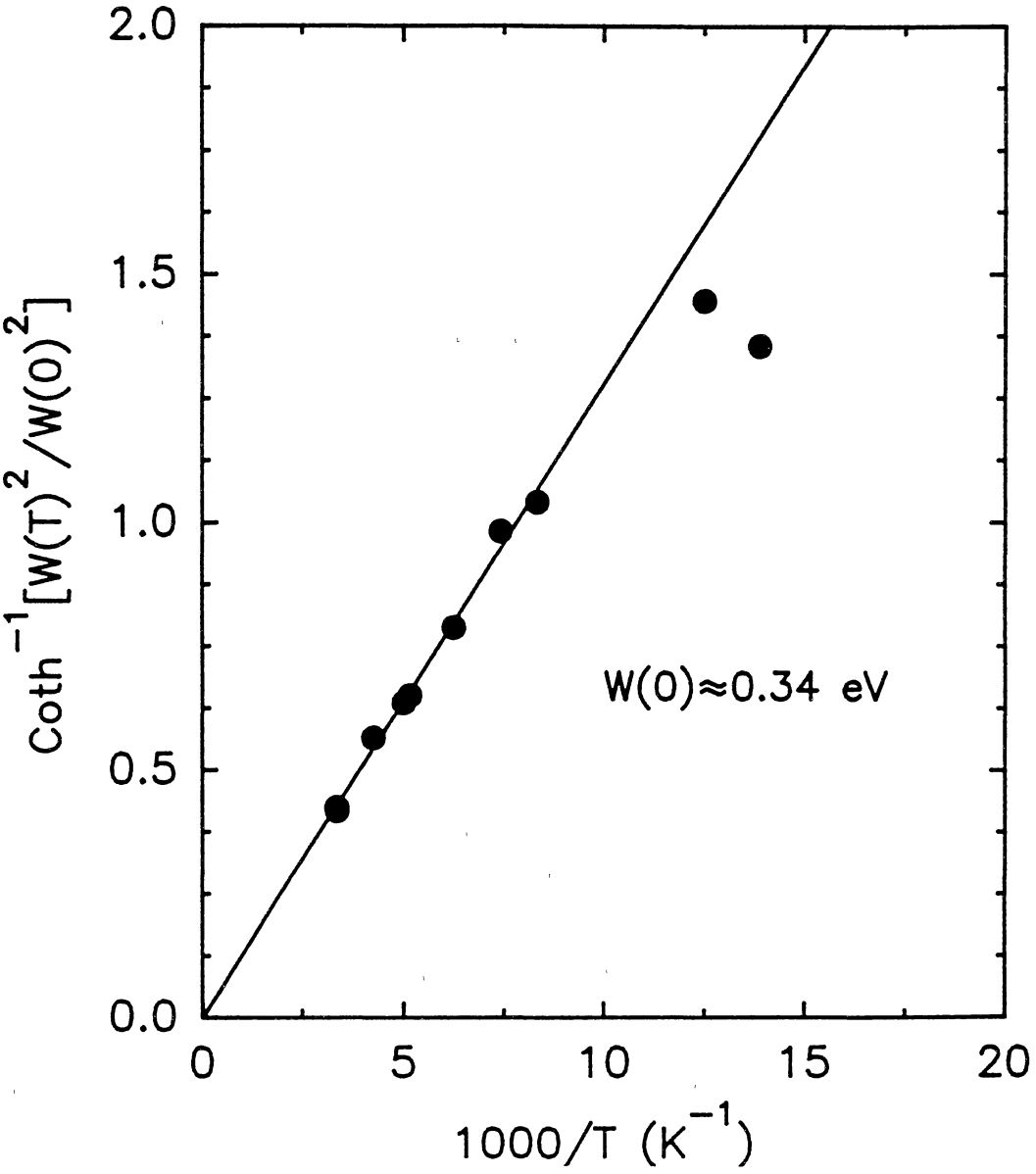


Figure 17. Temperature Dependence of the Width at Half-Maximum of the $\vec{E} \| c$ 3.7 eV F-center Absorption Band

effective frequency is dominant at the center.

From the slope of the line the effective frequency obtained is $5.34 \times 10^{12}$ Hz. Using the expression for W(0), the Huang-Rhys factor is found to be 43. This value is comparable to the Huang-Rhys values obtained for the F-center in the alkali halides for which S ranges from 20-40. From the model for the F-center, the Stoke's shift of the emission band relative to the absorption band is $2S\hbar\nu$. Though this emission band was not looked for in this study, it is expected to be centered about 1.81 eV (685 nm).

## The M-center in Lithium Yttrium Fluoride

At corresponding doses, the maximum absorption coefficients of the $\vec{E} \perp c$ 1.97 eV band are plotted versus the maximum absorption coefficients of the 3.7 eV F-center band in Figure 18. Again, the data plotted are the absorption coefficients obtained from the 77 K absorbance spectrum after irradiation at room temperature (300 K) and dry ice temperature (195 K). The two lines shown in the plot are the linear regressions of the data. The slope of the line obtained for the 300 K irradiation data is 1.84 and the slope of the line for the 195 K data is 2.04.

From this we see that both bands grow as the square of the F-center band. The simplest description for this band is that it is due to the M-center.

A plot of $\alpha_M$ versus $\alpha_F^2$ yields slopes of $9 \times 10^{-4}$ and $15 \times 10^{-4}$ for the 195 K and 300 K data, respectively. From

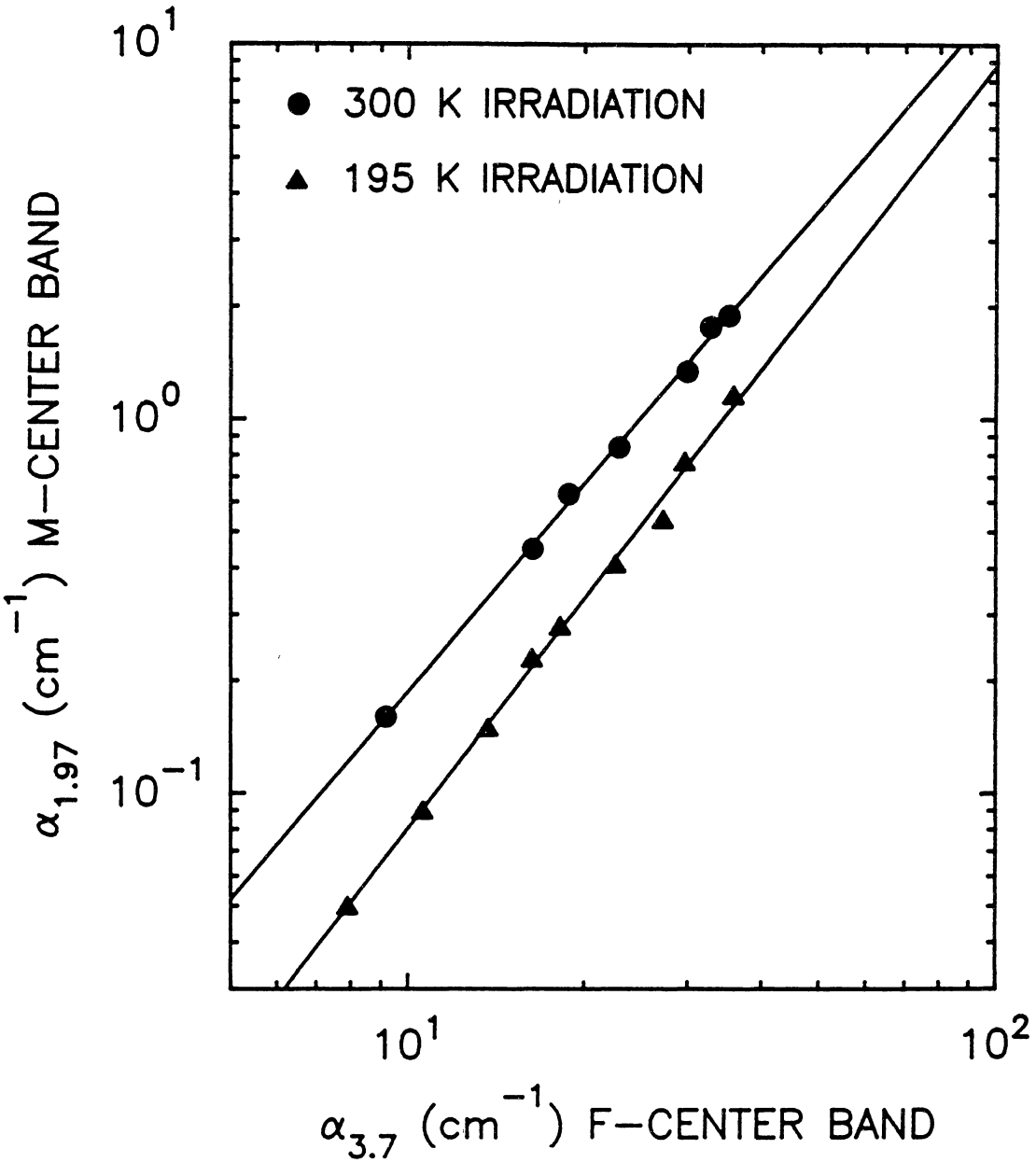


Figure 18. Absorption Coefficient of the $\vec{E}_{\perp}c$ 1.97 eV M-center Band as a Function of the Absorption Coefficient of the $\vec{E}\|c$ 3.7 eV F-center Band. The Absorption Coefficients were Measured at 77 K after Irradiation at 300 K and 195 K.

the expression for the slope, the number of neighbors which statistically contribute to M-center formation can be calculated using the appropriate constants of which only the oscillator strengths are unknown. Using values ranging from 0.4 to 2 for the ratio of $f_M/f_F^2$, K ranges from 5900 to 30000 for the 195 K irradiations and from 10000 to 51000 for the 300 K irradiations. High values for K are not unusual for high temperature irradiations and is taken as evidence of the contribution of thermal aggregation processes to M-center formation.[20]

Table II lists the maximum absorption coefficient and half-width at various temperatures for the 1.97 eV $\vec{E}_{\perp}c$ M-center band. The data were taken after room temperature electron irradiations to doses of $1.11 \times 10^{15}$ MeV/cm$^3$ and $1.41 \times 10^{15}$ MeV/cm$^3$ for the upper and lower sets of data respectively.

For this band we see consistency in the product of the maximum absorption coefficient and half-width at all temperatures, agreement in the half-widths at corresponding temperatures, and consistent values of the half-widths at low temperatures.

Figure 19 shows the plot of $\coth^{-1}[W(T)^2/W(0)^2]$ versus 1000/T with W(0) taken to be the average value of the 9 K half-widths. The straight line is the linear regression of the data obtained from 78 K and room temperature. The bestfit line does not intercept the origin as would be expected from the half-width equation. This deviation from

TABLE II

TEMPERATURE DEPENDENCE OF THE ABSORPTION COEFFICIENT AND THE WIDTH AT HALF-MAXIMUM OF THE 1.97 eV M-CENTER BAND WITH $\vec{E}_{\perp c}$

| TEMPERATURE (K) | ABSORPTION COEFFICIENT ($cm^{-1}$) | HALF-WIDTH (eV) | PRODUCT ($cm^{-1}$ eV) |
|---|---|---|---|
| 298 | 1.42 | 0.144 | 0.20 |
| 197 | 1.65 | 0.128 | 0.21 |
| 146 | 1.95 | 0.115 | 0.22 |
| 78 | 2.21 | 0.104 | 0.23 |
| 9 | 2.33 | 0.101 | 0.24 |
| 295 | 1.39 | 0.148 | 0.20 |
| 246 | 1.58 | 0.138 | 0.22 |
| 206 | 1.75 | 0.130 | 0.23 |
| 156 | 2.00 | 0.119 | 0.24 |
| 120 | 2.17 | 0.112 | 0.24 |
| 80 | 2.35 | 0.104 | 0.24 |
| 40 | 2.47 | 0.103 | 0.25 |
| 9 | 2.48 | 0.102 | 0.25 |

the theoretic expression for W(T) has also been found for the F-center in NaCl.[36] Taken as is, from the slope of the line, the calculated frequency is $5.99 \times 10^{12}$ Hz which is similar to value obtained for the 3.7 eV F-center band. This similarity in the frequencies has also been found in the alkali halides.[18,37] The value for the Huang-Rhys factor is found to be 3. At 0 K the transition probability for a zero-phonon transition is $W_{00}=\exp(-S)$. A high resolution scan over this absorption band at 9 K did not show a zero-phonon transition.

From the configuration coordinate model, an emission

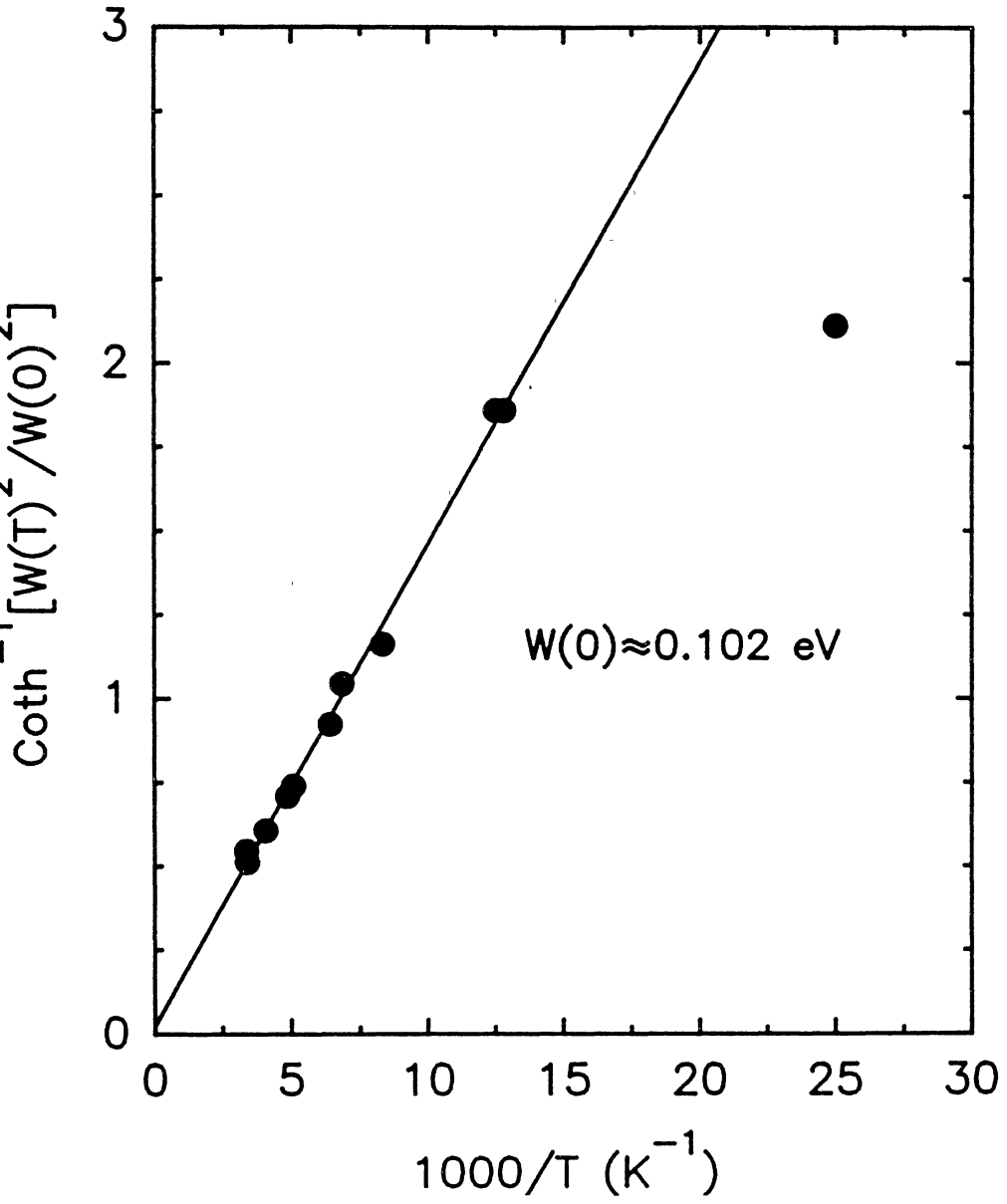


Figure 19. Temperature Dependence of the Width at Half-Maximum of the $\vec{E}\perp c$ 1.97 eV M-center Absorption Band

band associated with the $\vec{E}_{\perp c}$ 1.97 eV band should be centered about 1.82 eV (681 nm). As with the emission band for the F-center, this band was not looked for in this study.

## The R-center in lithium Yttrium Fluoride

Due to its low absorbance, and consequently its broadness, half-width data for the peak located at 2.3 eV were not accumulated. In Figure 20 the absorption data of the 2.3 eV band for the room temperature irradiations are plotted versus the absorption data of the 3.7 eV F-center band at corresponding doses (filled circles). The same data for 2.3 eV band are plotted versus the absorption coefficients of the 2.88 eV F-center band (filled squares).

The 300 K irradiation data has a slope of 2.95. Consequently this band grows as the cube of the F-center band and can be associated with the R-center. The slope of the line for the 195 K data changes continuously as the dose increases and only at the higher concentrations, larger values of absorption coefficient, does the data resemble what might be expected of the R-center.

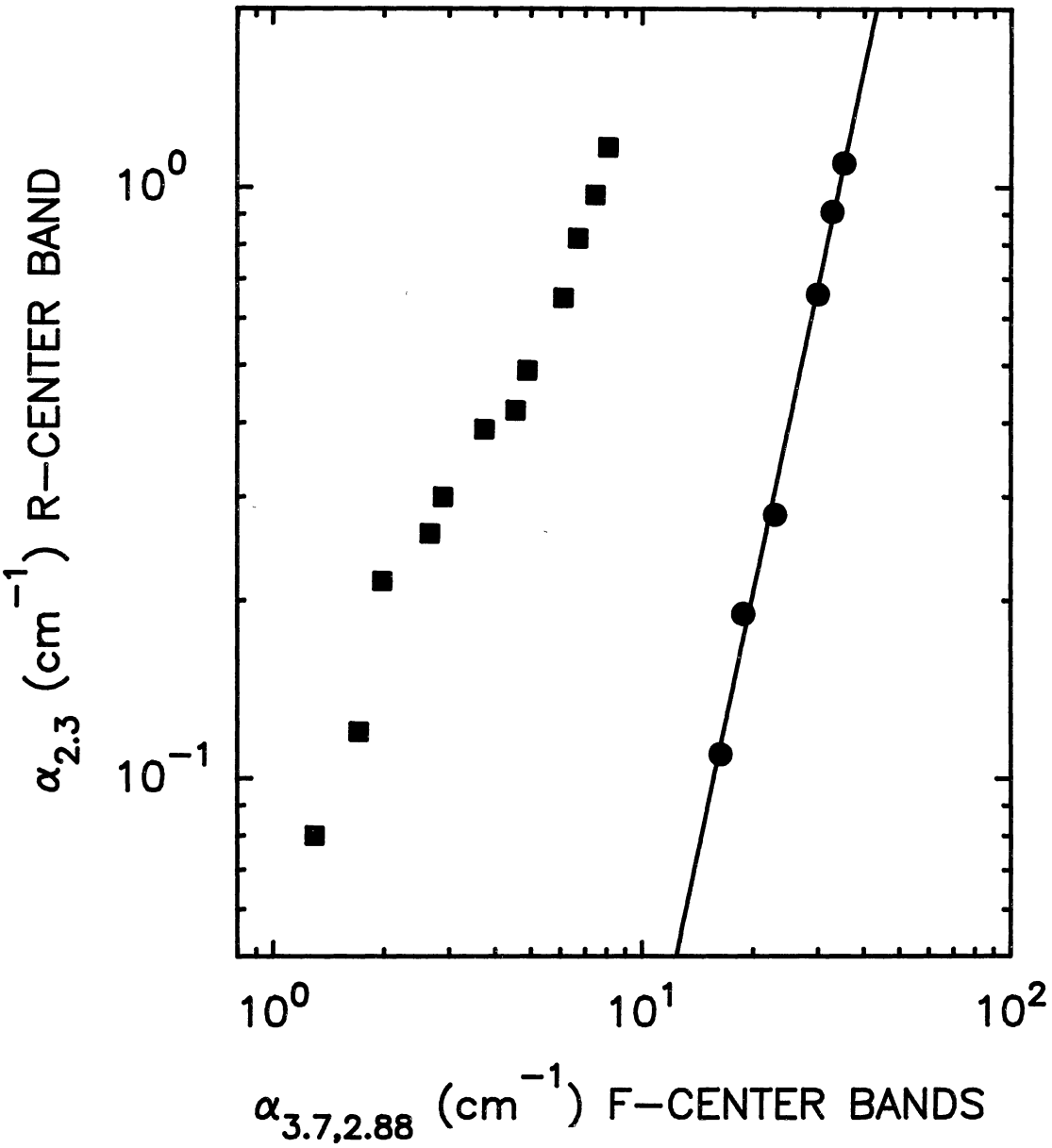


Figure 20. Absorption Coefficient of the $\vec{E}\perp c$ 2.3 eV R-center Band as a Function of the Absorption Coefficients of the $\vec{E}\parallel c$ 3.7 and $\vec{E}\perp c$ 2.88 eV F-center Bands. The Absorption Coefficients were Measured at 77 K after Irradiation at 300 K and 195 K.

# CHAPTER VII

## SUMMARY

The radiation induced absorption spectra of lithium yttrium fluoride has been measured for irradiation temperatures of 195 K and 300 K. Comparison of the optical spectra obtained after irradiation at the two different temperatures did not show a difference in the number and spectral location of the absorption bands at 77 K. The absorption bands observed at 1.96, 2.98, 3.7, and 4.94 eV were found to be polarized perpendicular to the c-axis. Other bands at 1.97, 2.3, 2.85, 3.7, and 4.43 eV were observed to be polarized parallel to the c-axis. The 3.7 eV band was found to be associated with the F-center by Renfro, et. al.

The half-width of the 3.7 eV F-center absorption band was measured at temperatures ranging from 9 to 300 K. For temperatures greater than 120 K these data obeyed the relation $W(T)^2 2 = W(0)^2 \coth(h\nu/kT)$ with the effective frequency $\nu$ equal to $5.34 \times 10^{12}$ Hz. The most probable transition of 3.7 eV was found to create 43 vibrational quanta (the Huang-Rhys factor). This is much too high for an observable zero-phonon transition. From these data an emission band associated with absorption in the spectral

range of the F-center absorption band is expected to be peaked at 1.81 eV. This band was not observed.

Two radiation-induced absorption bands, located at 2.85 eV (435 nm) and 4.43 eV (280 nm), were found to grow linearly with the 3.7 eV F-center band. It is apparent from the spectra that these two bands are polarized more strongly perpendicular to the c-axis, perpendicular to the 3.7 eV band. Hence, the simplest description for these two bands is that they are also due to the F-center.

The 1.97 eV absortion band was found to grow quadratically with the 3.7 eV F-center band and therefore has been identified as due to the M-center. The polarization data revealed this band is strongly polarized perpendicular to the c-axis. The half-width data of this band was measured from 9 K to 300 K. The data obtained for temperatures above 70 K obeyed the relationship $W(T)^2=W(0)^2\coth(h\upsilon/kT)$ with an effective frequency of $5.99x10^{12}$ Hz. From the data, a Huang-Rhys factor of 3 was determined. A high resolution absorbance scan over this band did not reveal a zero-phonon transition.

The room temperature irradiation data revealed the peak absorption coefficients of the 2.3 eV band varied as the cube of the 3.7 eV F-center peak absorption coefficients. Hence this band has been identified as due to the R or $F_3$ center. Half-width data for this weak, broad band were not accumulated.

## REFERENCES


1. Gabbe, D. and A. L. Harmer, J. Crystal Growth, **3,4**, 544 (1958).

2. Shand, W. A., J. Crystal Growth, **5**, 143 (1969).

3. Uhrin, R. and R. F. Belt, J. Crystal Growth, **38**, 38 (1977).

4. Thoma, R. E., C. F. Weaver, H. A. Friedman, H. Insley, L. A. Harris, H. A. Yakel, Jr., J. Phys. Chem., **65** 1096 (1961).

5. Brandle, C. D., Crystal Growth: A Tutorial Approach, Edited by W. Bardsley, D. T. J. Hurle and J. B. Mullin, North-Holland Publishing Company, (1979).

6. Woodruff, D. P., The Solid-Liquid Interface, Cambridge University Press, 1973.

7. Jani, M., private communication.

8. De Boer J. H., Rec. Trav. Chim., **56**, 301, (1937).

9. Billington, D. S. and J. H. Crawford, Jr., Radiation Damage in Solids, Princeton University Press, Princeton, New Jersey, 1961.

10. Billington, D. S., Editor, Radiation Damage in Solids, Academic Press, N. Y., 1962.

11. Chadderton, L. T., Radiation Damage in Crystals, Spottiswoode, Ballantyne & Co. Ltd., London, 1965.

12. Crawford, J. H., Jr., and L. M. Slifkin, Point Defects in Solids, Vol.1, General and Ionic Crystals, Plenum Press, N. Y., 1972.

13. Sonder, E. and W. A. Sibley, Chapter 4, p. 201, Point Defects in Solids, Vol.1, General and Ionic Crystals, Edited by J. H. Crawford, Jr., and L. M. Slifkin, Plenum Press, N. Y., 1972.

14. Crawford, J. H., Advan. Phys., **17**, 93 (1968).

15. Pooley, D., Solid State Communications, **3**, 241 (1965). Solids, **27**, 771 (1966).

16. Hersh, H. N., Phys. Rev., **148**, 928 (1966).

17. Castner, T. G. and W. Kanzig, J. Phys. Chem. Solids, **B3**, 178 (1957).

18. Konitzer, J. D. and H. N. Hersh, J. Phys. Chem., **32** 3, 843 (1960).

19. Renfro, G. M., L. E. Halliburton, W. A. Sibley, and R. F. Belt, J. Phys. C: Solid St. Phys., **13**, 1941 (1980).

20. Compton, W. D. and H. Rabin, Solid State Physics, Advances in Research and Applications, Edited by F. Seitz and D. Turnbull, **13**, Academic Press, (1964).

21. Smakula, A., Z. Physik, **59**, 603 (1930).

22. Faraday, B. J., H. Rabin and W. D. Compton, Phys. Rev. Letters, **7**, 57 (1961).

23. Thommen, K., Phys. Rev. Letters, **2**, 189 (1962).

24. Sibley, W. A. and E. Sonder, Phys. Rev., **128**, 540 (1962).

25. Riley, C. R. and W. A. Sibley, Phys. Rev. B, **1** 6, 2789 (1970).

26. Farge, Y. and M. P. Fontana, Electronic and Vibrational Properties of Point Defects in Ionic Crystals, North-Holland Publishing Co., (1979).

27. Engstrom, H. E., Phys. Rev. B, **11** 4, 1689 (1975).

28. Shand, W. A., J. Crystal Growth, **5**, 143 (1969).

29. Born, M. and J. R. Oppenheimer, Ann. Physik, **84** 457 (1927).

30. Fowler, W. B., Physics of Color Centers, Academic Press, N. Y., (1968).

31. Markham, J. J., F-Centers in Alkali Halides, Academic Press, N. Y., (1966).

32. Keil, T. H., Phys. Rev., **148** 2A, A601, (1965).

33. Huang, K. and A. Rhys, Proc. Roy. Soc. (London), **A204**, 403 (1950).

34. Gebhardt, W. and H. Kuhnert, Phys. Stat. Sol., **14**, 257 (1966).

35. W. L. Bond, Crystal Technology, John Wiley & Sons, Inc., (1976).

36. Markham, J. J. and J. D. Konitzer, J. Chem. Phys., **34** 6, 1936 (1961).

37. Rabin, H., Phys. Rev., **129**, 129 (1963).

# VITA

David Wayne Hart

Candidate for the Degree of

Doctor of Philosophy

Thesis: CRYSTAL GROWTH AND RADIATION-INDUCED DEFECTS OF RARE EARTH DOPED LITHIUM YTTRIUM FLUORIDE LASER HOST MATERIALS

Major Field: Physics

Biographical:

Personal Data: Born in Newton, Kansas, 8 December 1960, the son of Samuel C. and Delores S. Hart. Married Debra L. Stutsman, 3 August 1985.

Education: Graduated from Weatherford High School, Weatherford, Oklahoma, May 1979; received Bachelor of Science degree in Engineering Physics from Southwestern Oklahoma State University, Weatherford, Oklahoma, December 1984; received Master of Science degree in Physics from Oklahoma State University, May 1987; completed requirements for the Doctor of Philosophy degree at Oklahoma State University, December 1991.

Professional Experience: Laboratory Assistant, Department of Physics, Southwestern Oklahoma State University, August 1983 to December 1984; Teaching Assistant, Department of Physics, Oklahoma State University, January 1985 to May 1985; NASA Fellowship, July 1988 to July 1991; Research Assistant, Department of Physics, Oklahoma State University, June 1985 to Present.